Cerebral Cortex July 2010;20:1556-1573
doi:10.1093/cercor/bhp218
Advance Access publication October 7, 2009

Synchronization Dynamics in Response to Plaid Stimuli in Monkey V1

Bruss Lima, Wolf Singer, Nan-Hui Chen and Sergio Neuenschwander

Max-Planck Institute for Brain Research, 60528 Frankfurt am Main, Germany

Downloaded from cercor.oxfordjournals.org at Stadt und Universitatsbibliothek / Section Medizinische Hauptbibliothek on November 12, 2010

Gamma synchronization has generally been associated with grouping processes in the visual system. Here, we examine in monkey V1 whether gamma oscillations play a functional role in segmenting surfaces of plaid stimuli. Local field potentials (LFPs) and spiking activity were recorded simultaneously from multiple sites in the opercular and calcarine regions while the monkeys were presented with sequences of single and superimposed components of plaid stimuli. In accord with the previous studies, responses to the single components (gratings) exhibited strong and sustained gamma-band oscillations (30–65 Hz). The superposition of the second component, however, led to profound changes in the temporal structure of the responses, characterized by a drastic reduction of gamma oscillations in the spiking activity and systematic shifts to higher frequencies in the LFP (~10% increase). Comparisons between cerebral hemispheres and across monkeys revealed robust subject-specific spectral signatures. A possible interpretation of our results may be that single gratings induce strong cooperative interactions among populations of cells that share similar response properties, whereas plaids lead to competition. Overall, our results suggest that the functional architecture of the cortex is a major determinant of the neuronal synchronization dynamics in V1.

Keywords: attention, gamma, gratings, oscillation, visual cortex

Introduction

A major challenge in understanding perceptual organization is to explain how stable relationships are constructed dynamically in a multidimensional feature space. Given the distributed nature of cortical networks, an important goal is to identify the mechanisms by which selective neuronal interactions enable large-scale coordination of neuronal activity (Varela et al. 2001; Buzsáki and Draguhn 2004). Theoretical and experimental work suggests that temporal relationships in neuronal activity may serve as a linking mechanism for perceptual binding (reviewed in Gray 1999; Singer 1999; Engel et al. 2001). According to this concept, cell assemblies dynamically formed by synchronization of spiking activity constitute stable functional units, which allow for feature grouping processes, such as the pre-attentive segmentation of a visual scene (Gray et al. 1989; Engel et al. 1991; Kreiter and Singer 1996).

To validate this hypothesis, a general experimental goal has been to search for correlations between synchronously firing neuronal ensembles and perceptually coherent objects, such as moving bars, gratings, and dots (Gray et al. 1989; Engel et al. 1991; Eckhorn et al. 1993; Kreiter and Singer 1996; Palanca and DeAngelis 2005; Woelbern et al. 2002). In the majority of studies in which such correlations have been found, synchronization is typically accompanied by rhythmic activity in the gamma frequency band (30–90 Hz). This has been observed for spiking activity of single cells (single-unit activity, SUA) and small neuronal clusters (multi-unit activity, MUA), as well as for mesoscale signals, such as the local field potential (LFP), the electroencephalogram (EEG), and the magnetoencephalogram (Tallon-Baudry and Bertrand 1999; Varela et al. 2001; Vidal et al. 2006; Sehatpour et al. 2008). Gamma oscillations in the LFP generally show precise phase-locking to local spiking activity (König et al. 1995a), suggesting that the temporal structure carried by oscillatory signals represents an important synchronizing mechanism (Womelsdorf et al. 2007; Fries et al. 2008). Moreover, it has been shown that selective attention is associated with synchronization of oscillatory responses specifically at the gamma band (Müller et al. 2000; Fries et al. 2001; Taylor et al. 2005; Womelsdorf et al. 2006; Womelsdorf et al. 2007; Fries et al. 2008), which may serve as a mechanism for selective communication within and across cortical areas (Fries 2005; Fries et al. 2007).

In a previous study in the visual cortex of anesthetized cats, we have used superimposed drifting gratings (plaids) to investigate the role of synchronization on surface segmentation (Castelo-Branco et al. 2000a). Plaid stimuli are ideal to study visual segmentation because perception can be biased in a predictive manner by the manipulation of the luminance of the intersections, from 2 surfaces sliding on top of each other (noncoherent motion) to a single surface moving in an intermediate direction (coherent motion) (Stoner and Albright 1996). Furthermore, periodic stimuli such as plaids allow for a sustained activation of the cells, which was not possible to obtain in the previous conflicting bar studies (Gray et al. 1989; Engel et al. 1991; Kreiter and Singer 1996). From the results of Castelo-Branco et al. (2000a), synchronization of responses appeared to be dependent not only on the characteristics of the stimulus but also on similarity of receptive field (RF) properties. If the recorded neurons shared the same direction preferences and had either overlapping or colinear RFs, correlated activity was present for both the coherent and the noncoherent motion of the stimulus, indicating that the neuronal responses were associated to the contours of only one of the components. On the other hand, cell pairs showing large dissimilarities (direction preferences larger than 20° and noncolinear RFs) exhibited response synchronization only for the coherent motion of the plaids. Overall, these findings support the notion that neuronal synchronization contributes to surface segmentation, in accordance with the binding-by-synchronization hypothesis.

A direct test for neuronal correlates of perception can, however, only be approached by a behavioral paradigm. To address this problem, Thiele and Stoner (2003) trained one

© 2009 The Authors
This is an Open Access article distributed under the terms of the Creative Commons Attribution Non-Commercial License (http://creativecommons.org/licenses/by-nc/2.5/uk/) which permits unrestricted non-commercial use, distribution, and reproduction in any medium, provided the original work is properly cited.

monkey to report the motion coherence of plaid stimuli. In disagreement with the study of Castelo-Branco et al. (2000a), correlation analysis of single- and multi-unit responses in the middle temporal area (MT) showed no consistent relations with motion coherence, at odds with the predictions of the binding-by-synchrony hypothesis (Singer 1999; Engel et al. 1991; Kreiter and Singer 1996). Several other studies in behaving monkeys also failed to find evidence that synchronous firing correlates with contour integration (Roelfsema et al. 2004; Palanca and DeAngelis 2005).

To reexamine this controversial issue, we recorded simultaneously the LFP and spiking activity from V1 in response to plaid stimuli of monkeys performing a behavioral task. In contrast to the classical approach introduced by Movshon et al. (1985), our stimulus paradigm consisted in presenting sequentially single and superimposed components within the same trial. Thus, we were able to follow the synchronization dynamics of responses to stimuli that were likely perceived as coherent (one moving grating) and noncoherent (2 independently moving gratings), respectively. To sample from distributed populations of neurons, recordings were made simultaneously at the central and peripheral representation of the visual field. Essentially, 2 reasons motivated our study. First, it is well established that neurons in monkey V1 exhibit robust, sustained, synchronous oscillations in response to drifting gratings (Friedman-Hill et al. 2000; Maldonado et al. 2000). Thus, plaid stimuli should be particularly suited to study context-dependent synchronization phenomena. Second, in our study in the cat, as in most previous studies in the monkey (Kreiter and Singer 1996; Friedman-Hill et al. 2000; Maldonado et al. 2000; Thiele and Stoner 2003), only spiking responses have been taken into account, despite the fact that oscillations in the LFP are known to be very informative about interactions within cortical networks (Gray and Singer 1989; Frien et al. 2000, 2001; Siegel and König 2003; Kayser et al. 2003; Gail et al. 2004; Taylor et al. 2005; Henrie and Shapley 2005; Niessing et al. 2005; Liu and Newsome 2006; Belitski et al. 2008; Berens et al. 2008).

In the present study, we compared the spectral characteristics of LFP and spiking responses with single and superimposed components of plaid stimuli. The responses to single components were often associated with stable and strong gamma oscillations, in accordance with previous studies (Frien and Eckhorn 2000; Friedman-Hill et al. 2000; Gail et al. 2004). The appearance of the second component (plaid stimuli), however, led to cessation of the ongoing oscillatory patterning of the responses, independent of changes in rates. The disruption of gamma synchronization in the spiking responses coincided with a systematic shift of oscillation frequencies in the LFP. These changes in synchronization dynamics were not correlated with perceptual coherence, even when the monkeys were required to selectively attend to one of the components. As discussed below, our findings make it unlikely that the binding of local features relevant for scene segmentation takes place in V1, which is probably accomplished in higher areas.

Materials and Methods

Training and Visual Paradigm

Four rhesus monkeys (*Macaca mulatta*) participated in this study. Experimental procedures were approved by the German local authorities (Regierungspraesidium, Hessen, Darmstadt) and were in full compliance with the guidelines of the European Community for the care and use of laboratory animals (European Union directive 86/609/EEC).

Initially, the monkeys were trained on a fixation task. Each trial started with the appearance of a 0.15° square red fixation point (4 × 4 pixels; luminance, 10.0 cd/m^2), on which the monkeys were required to press a lever in the following 700 ms, and to maintain their gaze within a small virtual window (~1° × 1°) centered on the fixation point. In a random time point between 2500 and 4000 ms after fixation onset, the color of the fixation point changed from red to green. To obtain a reward, the monkey had to release the lever within a window of 200–500 ms after the color change of the fixation point. Trials were aborted when early or late lever releases occurred or whenever fixation was interrupted. For all aborted trials, a penalty pause of 2000 ms was added to the intertrial interval of 2000 ms, a period during which the animal was presented with a blank screen. Eye position was monitored continuously by a search coil system (DNI, Crist Instruments, USA; temporal resolution of 2 ms) or by an infrared eye tracker (Matsuda et al. 2000; temporal resolution of 33 ms). Typically, monkeys performed between 700 and 1500 correct trials in a 4-h session, thereby receiving their daily liquid requirement.

Stimuli were generated as sequences of bitmap images using an interface developed in LabVIEW by one of the authors (S.N.; LabVIEW, National Instruments, USA) and were presented as 1024 × 768 pixel resolution movies running at 100 or 120 frames per second using a standard graphical board (GeForce 6600-series, NVIDIA, Santa Clara, CA) controlled by ActiveStim (www.activestim.com). This software allowed high timing accuracy and stimulus onset jitters below 1 ms. The cathode ray tube monitor used for presentation (CM813ET, Hitachi, Japan) was gamma corrected to produce a linear relationship between output luminance and gray values and subtended a visual angle of 36° × 28° (1024 × 768 pixels).

At the beginning of each recording session, RFs were mapped using an automatic procedure in which a bar was moved across the screen in 16 different directions (n = 160 trials). RF maps were obtained by computing an average matrix, in which the responses were added in 10 ms bins (corresponding to 0.2° in visual angle) for all directions (see examples in Fig. 7*A*). The test stimuli that were subsequently presented consisted of moving gratings and plaid stimuli. The gratings (or single components) had spatial frequency ranging from 1.25 to 2.0 cycles per degree and velocity ranging from 1.0 to 1.5°/s (orthogonal to their orientation). These values were chosen because they elicited robust average responses in V1 (see example in Supplementary Fig. 4). The gratings were square-wave functions and had a duty cycle of 0.3. The plaids (or 2 superimposed components) were constructed by superimposing 2 gratings with an offset of 135° in their moving direction (45° orientation offset).

Plaid transparency was manipulated by varying the luminance of the individual components and their intersections (range, 1.0–32.0 cd/m^2 on a scale from 0.05 to 1.0; stimulus mean luminance, ~14.0 cd/m^2). In this way, plaids could be perceived either as a single moving surface (pattern plaids) or 2 segregated surfaces drifting in different directions (depth-ordered and transparent plaids). For most of the experiments shown in this study, the depth-ordered configuration was used. Component 1, of higher luminance (~20.0 cd/m^2), was superimposed on component 2 (~8.0 cd/m^2). The visual stimulus extended from 4° to 16.0° of visual angle and was positioned at the average of the RF centers for all recorded neurons (see example in Fig. 6*A* for 2 RFs at the central and peripheral representation of the visual field).

Two behavioral paradigms were used in this study: 1) fixation point color change detection and 2) selective attention to one of the components of the plaids. For task (1) the monkeys were required to hold their gaze for 3200 ms on the fixation point and respond to a change in its color. The stimulus (irrelevant for the task) was always presented 800 ms after fixation onset and consisted of one of the following sequences: gratings-plaids, plaids-gratings, gratings-plaids-gratings, or plaids-gratings-plaids. Transition between stimuli occurred at 2000 ms for the sequences of 2 stimuli and at 1600 and 2400 ms for the sequences of 3 stimuli (points in time relative to fixation onset). A total of 16 motion directions (steps of 22.5°) were randomly presented within protocols of 320 trials. To assure artifact-free transitions within

Downloaded from cercor.oxfordjournals.org at Stadt und Universitatsbibliothek / Section Medizinische Hauptbibliothek on November 12, 2010

a sequence, changes between gratings and plaids were implemented by a dynamical color table assignment method. Note that component 1 remained unchanged throughout the sequences presented, because it was always placed on the foreground.

In the selective attention task, one monkey was trained to attend to a luminance increase (~25%) of one of the components of a depth-ordered plaid. In this task, the fixation point remained unchanged and served only to hold the monkey's gaze. The grating to which attention had to be directed (cue grating) appeared first on the screen for a duration of 1000 ms. The second grating (distractor) was then displayed in front or behind the first. After 1000 ms, the luminance change occurred on either of the components with equal probability. The monkey was required to respond immediately to the luminance change of the cued grating. In case the luminance change occurred for the distractor grating, the monkey was required to wait another 1000 ms until the cued grating finally changed. Only the first plaid window (before any luminance increase occurred) was considered for further analysis. In this case the stimulus was physically the same, but attention could be directed to either of its surfaces.

Preparation and Recording Procedures

Each monkey was surgically implanted with a titanium bolt for stabilizing head position, a scleral search coil for measuring eye position, and a titanium recording chamber (internal diameter, 6 mm) that allowed microelectrode access to V1. The titanium pieces were fixed to the skull by means of orthopedic screws (Synthes, Germany) according to the methodology developed by N. K. Logothetis and collaborators at the Max-Planck Institute for Biological Cybernetics. All surgical procedures were conducted under aseptic conditions with isofluorane anesthesia (Baxter, Germany) and assisted by a pressure-controlled ventilation unit (1.8 l/min N_2O and 0.8 l/min O_2; Julian Station, Dräger Medical, Germany).

Recordings were made from the opercular region of V1 (RFs centers, 2.0°–3.0° eccentricity) and, occasionally, from the superior bank of the calcarine sulcus (10.0°–13.0° eccentricity). Electrodes were inserted independently into the cortex via guide tubes positioned above the dura (diameter, 300 μm; Ehrhardt Söhne, Germany) assembled in a customized recording device (designed by S.N.). This device comprised 5 precision hydraulic microdrives mounted onto an X–Y stage (MO-95, Narishige Scientific Instrument Laboratory, Japan), which was secured onto the recording chamber by means of a screw mount adapter, thereby providing great recording stability. Quartz-insulated tungsten–platinum electrodes (Thomas Recording, Germany; diameter, 80 μm) with impedances ranging from 0.3 to 1.0 MΩ were used to record simultaneously the extracellular activity from 4 to 5 sites in both superficial and deep layers of the cortex.

Data Collection and Spike Sorting

Spiking activity of small groups of neurons (MUA) and the LFP were obtained by amplifying (1000×) and band-pass filtering (MUA, 0.7–6.0 kHz; LFP, 0.7–170 Hz) the recorded signals with a customized 32 channels Plexon pre-amplifier connected to an HST16o25 headset (Plexon Inc., USA). Additional 10× signal amplification was done by onboard amplifiers (E-series acquisition boards, National Instruments, USA). The signals were digitized and stored using a LabVIEW-based acquisition system developed in our laboratory (SPASS, written by S.N.). LFP was acquired with a resolution of 1.0 ms. Spikes were detected by amplitude thresholding, which was set interactively after online visualization of the spike waveforms (typically, 2–3 standard deviations above noise level). Spike events and corresponding waveforms were sampled at 32 kS/s (spike waveform length, 1.2 ms).

Off-line spike sorting was performed using a dynamic template matching method implemented in a custom software package (SpikeOne, developed by N-H.C.). Sorting was initiated by an automatic procedure that defined up to 12 different clusters. Various displays, such as tuning curves, autocorrelograms, and measurements of recording stability, were used to guide interactively which cluster to merge or delete. Only clusters well separated in 2D and 3D plots of spike principal component analysis scores were assigned to single-units (SUA) if a refractory period was confirmed in interspike interval distributions.

Data Analysis

Our analysis consisted essentially in obtaining measures of temporal patterning for local (SUA and MUA) and global (LFP) neuronal activity in V1. To maximize the insight into the data, both time domain and frequency domain approaches were used. For assessment of synchronous oscillations in MUA responses, auto- and cross-correlograms were computed on a trial-by-trial basis (resolution, 1.0 ms; time shifts, 80 ms) and then averaged over 15–20 repetitions for each stimulation condition. Shuffled cross-correlograms (shift predictors) were also routinely computed to control for correlations resulting from phase-locking to the stimulus onset. Because the shift predictors were always flat, they were not subtracted from the raw correlograms. A damped cosine function was fitted to the correlograms as described by König (1994) and used to extract 2 modulation amplitude ratios: one associated with the first satellite in the correlograms, which estimates the strength of oscillatory modulation, and the other one associated with the central peak, which estimates the strength of response synchronization. Peaks were measured from the offset of the fitted function, and the confidence limit for the statistical significance of their values was established as follows: Gabor fits had to account for ⩾15% of the data variance and the *z*-scores of significant peaks had to be >2.

Spectral quantities were estimated for both spike and LFP signals using the multitaper method (Thomson 1982) implemented in Chronux 2.0 (Mitra and Bokil 2008), an open-source, MATLAB-based (Mathworks Inc., Natick, USA), data analysis toolbox available at http://chronux.org. Essentially, the multitaper method attempts to reduce the variance of spectral estimates by pre-multiplying the data with several orthogonal tapers known as Slepian functions. The frequency decomposition of multitapered data segments therefore provides a set of independent spectral estimates that, once averaged, provides an ensemble estimate that is more reliable for noisy data.

Mathematically, the multitapered power spectrum of a time series is defined for a given frequency as an average over all repetitions and tapers:

$$s_x(f)=\frac{1}{K}\sum_{k=1}^{K}\left|\tilde{x}_{n,k}(f)\right|^2,$$

where

$$\tilde{x}_{n,k}(f)=\frac{1}{N}\sum_{n=1}^{N}e^{-i2\Pi ft}w_k(t)x_n(t),$$

is the discrete Fourier transform of the product of the measured time series sequence $\{x_n(t),\ n = 1, 2, \ldots, N\}$ with the *k*-th Slepian taper, denoted $w_k(t)$. Numerically, $\tilde{x}_{n,k}(f)$ is computed as the Fast Fourier transform of the product. Data segments of 700 ms and 800 ms were padded with zeros to the length of 2048 before the Fourier transformation. Five Slepian tapers were used for both spike and LFP data. Hence, we obtained a spectral concentration of ±4.28 Hz and ±3.75 Hz for the data segments of 700 ms and 800 ms, respectively. For computation of the spectrograms, we used windows of 200 ms displaced at 50-ms steps. For this case, the spectral concentration was ±15 Hz.

The degree of synchronous oscillations between pairs of time series was also evaluated by computing a frequency domain measure known as coherence, defined as:

$$C_{yx}(f)=\frac{\left|S_{yx}(f)\right|}{\sqrt{S_x(f)S_y(f)}},$$

where $S_x(f)$ and $S_y(f)$ are the multitapered power spectrum estimates of the time series $x_n(t)$ and $y_n(t)$ averaged over n repetitions, respectively, and $S_{yx}(f)$ is the cross-power of these 2 time series. Coherence provides a normative measure of linear association between 2 processes on a scale from 0 to 1. In the absence of noise, a coherence value of 1 will be obtained at all frequencies if 2 processes are linearly related, that is, their amplitude covary and they maintain a constant phase relationship. If the 2 processes are independent, coherence will be equal to 0.

The 95% confidence bounds about spectral estimates were determined by the jackknife method across tapers and trials. A similar procedure was used to determine significant differences between 2 coherence measures (Arvesen jackknife test). Both tests were

Downloaded from cercor.oxfordjournals.org at Stadt und Universitatsbibliothek / Section Medizinische Hauptbibliothek on November 12, 2010

implemented in the Chronux software package. Two analysis windows of 800 ms were positioned 200 ms after each stimulus onset for the sequences gratings-plaids and plaids-gratings. For the sequences gratings-plaids-gratings and plaids-gratings-plaids, windows of 700 ms were positioned 100 ms after the onset of the first 2 stimuli (the third stimulus in the sequence was discarded). The power spectrum measures were computed in z-score units relative to the spontaneous activity. Essentially, for each frequency bin and stimulus condition, the power spectrum of the baseline activity (epoch between fixation onset and stimulus onset) was subtracted from the power spectrum of the induced activity and divided by the standard deviation of the baseline activity (for the baseline activity, trials of all stimulus conditions were considered). A recording site was considered to have significant gamma oscillations if at least one bin in the frequency range between 30 and 90 Hz showed z-score value greater than 1.96 (95% threshold) for the preferred condition (stimulus condition where component 1 yielded the highest firing rate). To access significant differences in coherence measures, the same procedure was applied, but using the Arvesen jackknife test instead of the z-score. The preferred condition, consisting of the gratings (component 1) and plaids (component 1 + 2) stimuli, was considered for further analysis. The LFP spectrum is displayed in z-score units, whereas the MUA spectrum is displayed as power divided by firing rate for the same analysis window (Pesaran et al. 2002). Because both are normalized measures, responses from different recording sites could be directly pooled for population analysis. For visualization purposes in the single case plots, spectral quantities were smoothed with a cubic spline function (smoothing parameter $p = 0.1$).

Group data were compared by t-tests (paired and independent sample) and analysis of variance (ANOVA) (repeated and nonrepeated measures). Fisher's least significant difference test was used for multiple comparisons among means. Significant levels were set at 95% ($P < 0.05$).

Results

MUA and LFPs were acquired with multiple-electrode recordings from area V1 in 7 hemispheres of 4 macaque monkeys. For selected recording sites spike sorting of the MUA was performed in order to obtain SUA. All monkeys were trained to maintain fixation and to respond to a color change of the fixation point (correct trials, Monkey 1, 96%; Monkey 2, 80%; Monkey 3, 96%; Monkey 4, 90%). One monkey (Monkey 3) was trained in addition to attend to one of 2 superimposed moving gratings and to report a luminance change of that grating. Quantitative RF mapping and direction tuning curves were computed for all recorded sites.

A total of 471 recording sites across 109 sessions were obtained. Of these, 411 sites were located in the opercular region and 60 in the calcarine sulcus of V1, representing eccentricities in the visual field of approximately 3° and 10°, respectively. This gave rise to 737 cross-electrode recording pairs, 551 of which were pairs across operculum sites, 44 were pairs across calcarine sites, and 142 were pairs across operculum and calcarine sites. For the MUA, 89% of the sites showed significant responses to at least one of the 16 oriented moving gratings presented over their RFs ($P < 0.05$, 2-tailed z-score relative to the spontaneous activity). With the exception of 3 cases, all recordings exhibited an increase of firing rates in response to the stimulus.

Gamma Oscillatory Responses

Moving gratings with optimal orientation, spatial frequency, speed, and contrast are known to induce strong synchronous gamma oscillations visible in MUA, SUA, and the LFP (Gray and Singer 1989; Engel et al. 1990; Frien and Eckhorn 2000; Friedman-Hill et al. 2000). In accord with these studies, we have observed significant gamma oscillations in the LFP for responses to the preferred orientation for 99% of all recording sites ($P < 0.05$, 2-tailed z-score relative to the spontaneous activity; see Material and Methods for significance criteria). The incidence of gamma oscillations in the MUA for the preferred orientation was substantially lower. Only 14% of all sites recorded exhibited significant oscillations ($P < 0.05$). The data for the 7 hemispheres studied are summarized in Table 1.

Figure 1*A* gives an example of strong gamma oscillations in MUA responses to optimal gratings (oscillation frequency of 65 Hz, average modulation amplitude of 1.49). Strong oscillations were also visible in single-cell responses, with frequencies precisely matching the one for the MUA (65 Hz, modulation amplitudes of 0.88 and 1.14). Cross-correlation analysis revealed that nearby cells engaged in rhythmic synchronous firing (Fig. 1*B*, modulation amplitude of 2.40), indicating strong local interactions. Analysis of an additional cell, recorded 3-mm away from the first electrode, showed similarly strong synchronous oscillations at the same frequency (65 Hz, modulation amplitude of 1.53). Notice that this latter pair of cells also had similar orientation preferences. These results confirm early findings in the cat and in the monkey that cells sharing similar properties often exhibit strong synchronous oscillatory firing in response to optimally oriented stimuli (Engel et al. 1990; Maldonado et al. 2000).

Overall, the temporal characteristics of the gamma responses to gratings that we observed in the behaving monkey closely resembled those described previously in areas 17 and 18 of the cat (Eckhorn et al. 1988; Gray et al. 1990; Engel et al. 1990) and area V1 of the monkey (Eckhorn et al. 1993; Frien and Eckhorn 2000; Friedman-Hill et al. 2000; Rols et al. 2001).

Disruption of Ongoing Gamma Responses

If segmentation of plaid surfaces is accomplished in V1, neurons sharing similar properties should synchronize their activity in response to the same surface in a condition of perceptual segmentation (Castelo-Branco et al. 2000a). To test this idea, we developed a paradigm in which the onset of the second component of a plaid was delayed relative to the onset of the first component. Plaid stimuli were displayed with equal luminance values for the intersection and the first component, which were set to be higher than the one for the second component (depth-ordered plaids, as in Thiele and Stoner 2003). For this configuration, we expected that synchronous responses to component 1 should be maintained as the cells

Table 1
Recording sites with significant gamma oscillations for the MUA

	Monkey 1 (nic)	Monkey 2 (lili)	Monkey 3 (jeb)	Monkey 4 (kai)
In response to gratings				
Left hemisphere	0	31%	8%	5%
Right hemisphere	1%	1/1[a]	55%	—
In response to plaids				
Left hemisphere	0	2%	0	0
Right hemisphere	0	0	12%	—

[a]Significant MUA gamma oscillations for the gratings were observed for the only site recorded.

Downloaded from cercor.oxfordjournals.org at Stadt und Universitatsbibliothek / Section Medizinische Hauptbibliothek on November 12, 2010

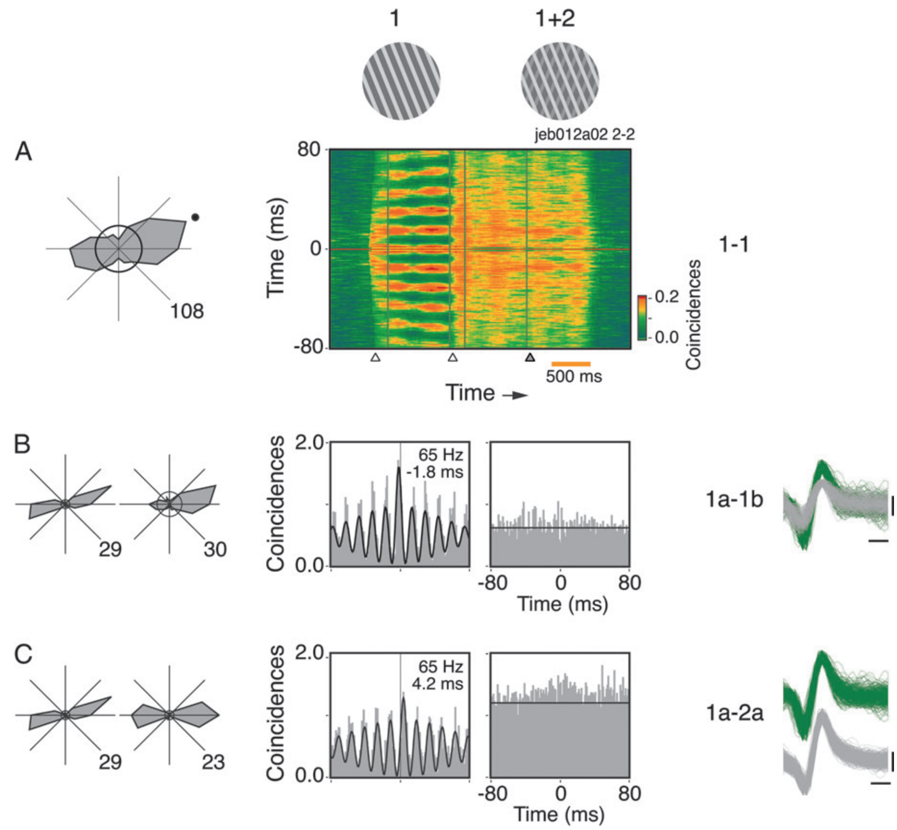

Figure 1. Examples of disruption in the oscillatory patterning of spiking responses to plaid stimuli (data obtained from Monkey 3). (*A*) The first component of the plaids (1), matching the preferred direction of the cells (black dot in the tuning curve, displayed to the left), induced strong gamma oscillations as seen from the sliding window autocorrelation analysis of the MUA. The onset of the second component of the plaid (1 + 2), presented behind the first, abolished almost completely the ongoing oscillatory patterning of the responses. The disruption effect was also visible in the cross-correlation analysis for single cells. Cross-correlograms obtained for a pair of cells with similar properties recorded from the same electrode (*B*), and for a pair of cells recorded from electrodes ~3-mm apart (*C*). Analysis windows are indicated by the boxes in (*A*). Spike waveforms of each isolated cell are displayed to the right. Maximum mean firing rate (spikes/s) is indicated at the right corner of each tuning curve. The circle in the center of the tuning curves represents the mean spontaneous rate. Stimulus timing events (onset of component 1, onset of component 2, and fixation point color change) are indicated by the arrow heads at the bottom of the sliding window panel. Oscillation frequency and phase shift indicated in the correlograms were obtained after fitting of a damped cosine function to the correlograms. Protocol identification labels are given at the top right-hand corner of the sliding window plot. The first 3 characters in the label identifies the monkey (nic corresponds to Monkey 1, lil corresponds to Monkey 2, and jeb corresponds to Monkey 3). The same convention is applied to all other Figures.

were still responding to this very surface. As shown in Figure 1, our results do not support this hypothesis. In this example, the neurons had overlapping RFs and shared similar orientation preferences (see tuning curves in Fig. 1). The strong gamma responses induced by component 1 alone (gratings, first window in the figure) ceased nearly completely after component 2 onset (plaids, second window). Notably, there were no signs of synchronization after the interruption of the oscillatory activity. Because disruption in gamma responses was observed also at the single-cell level, we could discard effects of recruitment of new cells contaminating the recorded MUA signal responding to the other component. Changes in firing rates are also unlikely to be an explanation. As demonstrated for the cell pair in Figure 1*B*, differences in the correlograms may be dramatic, despite negligible changes in rate.

As a control for effects related to the sudden onset of component 2, we have done experiments for which component 2 appeared gradually (Supplementary Fig. 1). This was important to rule out the effects of involuntary attentional capture by abrupt onsets as a possible explanation to our results. As shown in Supplementary Fig. 1, disruption in oscillatory patterning of the responses was clearly seen even when component 2 onset was void of transients.

In the LFP, the onset of component 2 led to a profound attenuation of oscillation strength in most of the cases. Moreover, these effects were systematically associated with shifts in oscillation frequency. As shown in the time–frequency analysis of Figure 2*A*, the strong and sustained oscillations induced by component 1 changed toward less sustained and weaker oscillations at a higher frequency. Note that the prominent 62-Hz peak for component 1 is shifted to 69 Hz after component 2 onset. The reduction in power of the LFP was ~54%, as measured for the entire gamma band (62% peak amplitude reduction). In this study, the spectral power of the LFP was estimated as a function of standard deviation units (*z*-score) of the spontaneous activity.

Figure 2*B* shows, for the same recording site, the disruption effect for the power of MUA responses. In this case, different from the example of Figure 1*A*, the disruption was not complete in the MUA. Nevertheless, the remaining oscillation does not appear to be a continuation of the oscillatory process initially triggered by the single component. There is a clear shift in oscillation frequency, of the same amount as the one observed for the LFP. The attenuation in gamma power was striking with a drop to about 33% (65% peak amplitude reduction). Cases in which the MUA gamma oscillations

Downloaded from cercor.oxfordjournals.org at Stadt und Universitatsbibliothek / Section Medizinische Hauptbibliothek on November 12, 2010

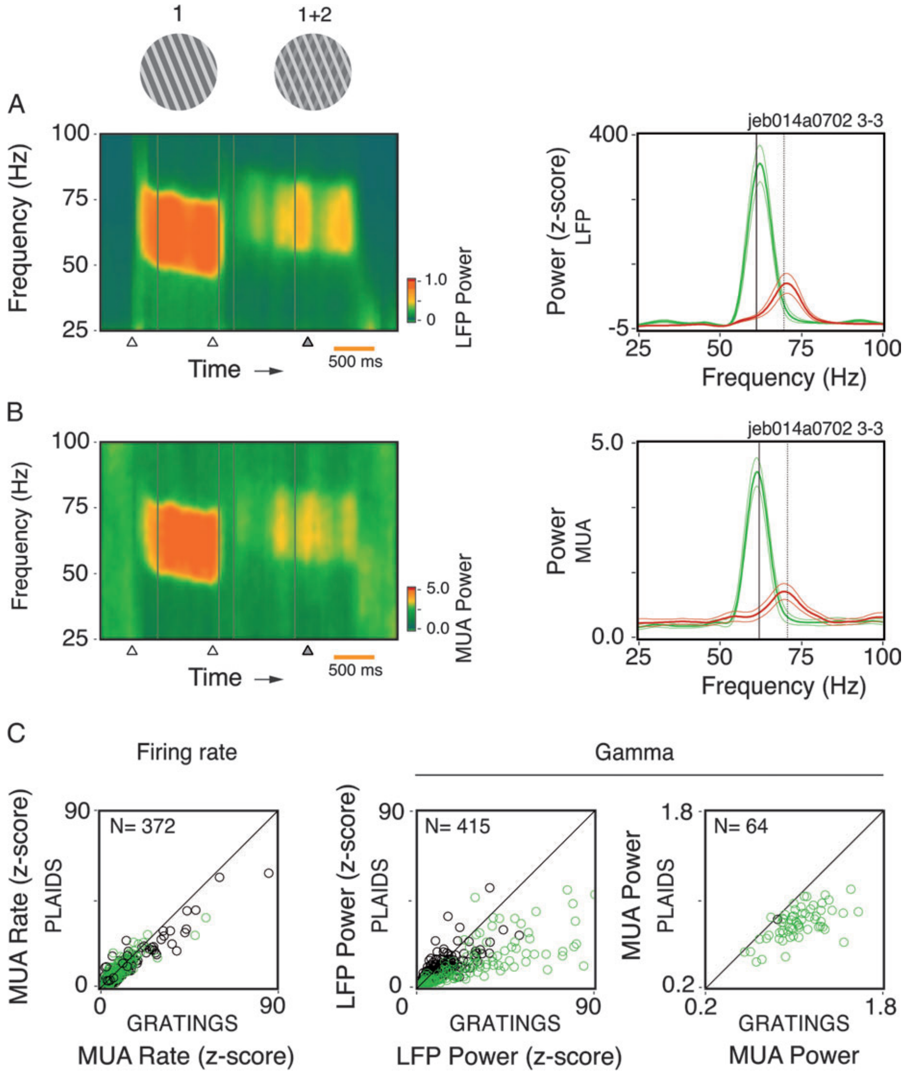

Figure 2. Spectral analysis for the LFP and MUA for responses to single (1) and superimposed components (1 + 2) of the plaid stimuli. (*A*) Time–frequency analysis and power spectrum computed for the LFP (e.g., from Monkey 3). The thick green and red traces represent single component (gratings) and 2 superimposed component stimuli (depth-ordered plaids), respectively, averaged over 24 trials. The thinner traces enclose the 95% confidence interval of the mean. Notice that the onset of component 2 led to reduction of gamma power and a shift toward higher oscillation frequency. (*B*) Spectral analysis for MUA, same recording as in (*A*). (*C*) Population data for rates, LFP gamma power, and MUA gamma power in response to single and superimposed grating components (depth-ordered plaids). Black circles represent recording sites from Monkey 1, whereas green circles represent recording sites from Monkeys 2, 3, and 4. Only those sites showing a significant increase in activity for component 1 relative to the baseline are plotted. Component 2 onset significantly reduced LFP gamma power (average of 54% decrease, paired *t*-test, df = 179, $P < 10^{-6}$) for Monkeys 2, 3, and 4. Monkey 1 showed only a weak effect (10% decrease, paired *t*-test, df = 234, $P = 0.017$). A significant reduction in MUA gamma power was also observed for all monkeys (24%, paired *t*-test, df = 63, $P < 10^{-6}$). On average, there was no significant change in the firing rates (paired *t*-test, df = 163, $P = 0.76$), with the exception of Monkey 1 (12% reduction, paired *t*-test, df = 207, $P < 10^{-5}$). Data shown correspond to the condition eliciting the strongest spiking response to component 1.

persisted after component 2 onset represented only a small fraction of our total sample (15% of the recording sites). Analysis at the population level confirmed the results above, despite a clear variability across monkeys (Fig. 2*C*). Notice that there are no strong signs of cross-orientation suppression when component 2 is added. The reason for this probably lies in the fact that in our study most of the stimuli had much higher luminance values for component 1 than for component 2. Taken together, the results obtained for the spiking responses and for the LFP indicate that in our paradigm component 2 induces a new network dynamics, disrupting the ongoing synchronization process. This happens even for cell pairs responding selectively to the same surface (Fig. 1*B*,*C*), in contradiction with our initial hypothesis. Additional analysis for all conditions tested is documented in Supplementary Results and Supplementary Fig. 2.

To further evaluate the impact of the second component on synchronization, coherence values were computed for the LFP–LFP and the MUA–MUA (across electrodes) and the LFP–MUA (from the same electrode and across electrodes) (Fig. 3). In the example shown in Figure 3*A*, consistent with the spectral analysis above, we observed a clear shift in frequency for all coherence measures (from 64 to 72 Hz), with particularly striking attenuation for the MUA–MUA and the LFP–MUA (65% and 52% decrease, respectively). For the LFP–LFP coherence, the attenuation effect was weak. Actually, in responses to the plaids, there was a clear dissociation in the oscillatory patterning between the LFP and MUA. As shown in

Downloaded from cercor.oxfordjournals.org at Stadt und Universitatsbibliothek / Section Medizinische Hauptbibliothek on November 12, 2010

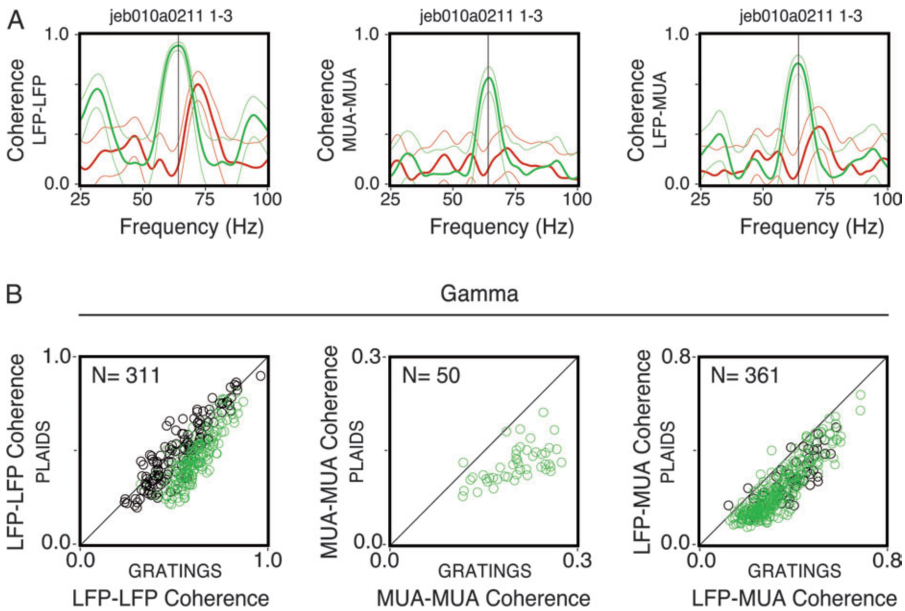

Figure 3. Coherence analysis. (*A*) Example of LFP–LFP, MUA–MUA, and LFP–MUA coherence measures for the grating (green) and plaid (red) stimuli derived from the same pair of recording sites (Monkey 3). Thin lines correspond to the 95% confidence interval (estimated by the jackknife procedure). (B) Population data for each of the corresponding coherence measures presented in (*A*). Black circles represent data points from Monkey 1, whereas green circles represent sites from Monkeys 2, 3, and 4. The number of site pairs for each analysis is given on the top left-hand side. Data shown correspond to the condition eliciting the highest joint firing rate response to component 1, as measured by the geometric mean for each pair of sites. Only those sites showing a significant increase in coherence for component 1 relative to the baseline are plotted. Plaids were depth-ordered.

Figure 3*A*, the phase-locking for the LFP–LFP was largely absent for the MUA–MUA and for the LFP–MUA. Notice that this dissociation effect was present for the plaids, but not for the gratings. Population data are shown in the scatter plots of Figure 3*B*. Only the recording pairs showing a significant increase in coherence for the preferred condition of the gratings are shown (310 out of 643 pairs for the LFP, 50 out of 643 pairs for the MUA, and 361 out of 1704 pairs for the LFP–MUA). For all monkeys, the coherence estimates exhibited a significant reduction (17% for the LFP, paired *t*-test, degrees of freedom [df] = 310, $P < 10^{-6}$; 35% for the MUA, paired *t*-test, df = 49, $P < 10^{-6}$; 29% for the LFP–MUA, paired *t*-test, df = 360, $P < 10^{-6}$). For the LFP–MUA, the reduction was more accentuated for recording pairs obtained from different electrodes as compared with pairs obtained from the same electrode (36% and 22%, respectively). Notice that this effect was less evident for the LFP coherence of Monkey 1 (5% reduction, paired *t*-test, df = 130, $P < 10^{-6}$). Furthermore, no recording pair for this monkey showed a significant increase in the MUA coherence. This is not unexpected because Monkey 1 rarely showed any rhythmic spiking responses and hence low coherence even for single gratings. It is important to emphasize that coherence was strongly dependent on cortical distances. As shown in Supplementary Results and Supplementary Fig. 3, coherence values were extremely attenuated for recording pairs across the operculum and the calcarine sulcus.

To study parametrically the impact of component 2 on the gamma responses, we varied in 2 cases its luminance and angle offset relative to component 1 (Fig. 4, example from Monkey 2). As shown by autocorrelation analysis, increasing in a few steps the luminance of component 2 led to a complete disruption of the ongoing gamma activity in the MUA (relative luminance from 0.15 to 0.20, Fig. 4*A*). Changing systematically the relative direction of component 2 led to similar results. For direction offsets between the components greater than 20°, there was a complete disruption of gamma, as shown in the cross-correlograms of Figure 4*B*. This effect is particularly intriguing in view of the data currently available for the cortical–cortical connectivity. It has been shown that excitatory connections are biased for iso-orientation domains, within ±20° (Kisvárday et al. 1997; Malach et al. 1993). Interestingly, we have observed that gamma synchronization was not disrupted when the direction of component 2 was offset by 180° (opposing directions). In this particular condition, the orientation of the 2 components was the same, and the activated neurons shared similar orientation preferences (see Supplementary Fig. 2). Similar results were also obtained by Lamme and Spekreijse (1998) for opposing moving textured surfaces. These findings suggest that the disruption of gamma oscillations is caused by the coactivation of columns with differing orientation preferences rather than by the properties of the stimulus per se.

Shifts in Gamma Oscillation Frequency

As shown above, component 2 led in most of the cases to a reduction of the gamma responses in the LFP. Moreover, we observed systematic shifts in gamma frequency for all monkeys studied. This effect was independent of the attenuation in oscillation strength. In Figure 5, we show LFP data for the same stimulus paradigm described in the previous figure but obtained from a different monkey (Monkey 1). Small increments in component 2 luminance resulted in systematic shifts in the gamma oscillation peak (Fig. 5*A*). For a low luminance value the shift in frequency was negligible. For the next luminance steps, however, shifts in frequency were considerable, eventually reaching asymptote at 70 Hz. The same effect on frequency was also present when the relative direction of

Downloaded from cercor.oxfordjournals.org at Stadt und Universitatsbibliothek / Section Medizinische Hauptbibliothek on November 12, 2010

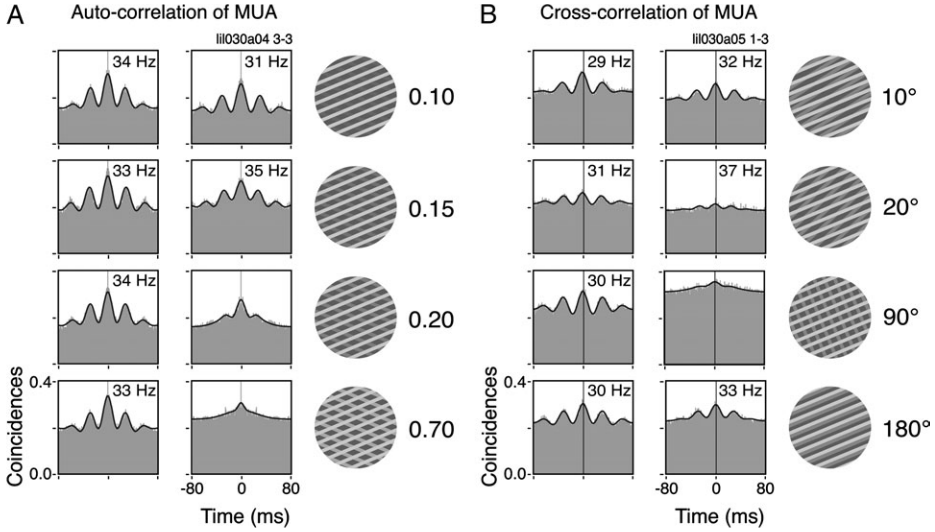

Figure 4. Parametric study on the disruption of the ongoing spike gamma oscillations. Correlograms for the single and superimposed components (depth-ordered plaids) are shown to the left and to the right of each panel, respectively. (*A*) Successive luminance increases of component 2 led to increasing attenuation of the spiking gamma oscillations. (*B*) Component 2 is presented in different directions of motion relative to component 1. The more orthogonal both components are, the higher the attenuation of spiking gamma oscillations. Note that very small increments of luminance (*A*) or relative direction difference (*B*) are sufficient to virtually abolish the oscillatory patterning of the responses.

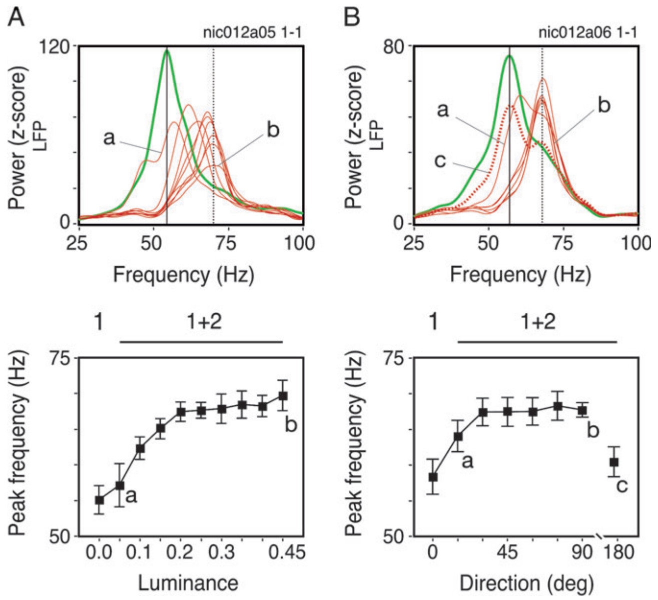

Figure 5. Gamma frequency shifts of LFP oscillations for the same experimental paradigm described in Figure 4. Green and red curves represent single and superimposed grating components, respectively. (*A*) Luminance increments of component 2 induced successive increases in the LFP gamma frequency, as represented by the thin red traces. (*B*) Relative angle deviations leading to more perpendicular crossings of both grating components similarly led to successively higher frequencies. The dotted red curve represents superimposed gratings with the same orientation but moving in opposite directions. For this case no frequency shift was observed. The panels below the power spectra plots depict the gamma frequency as a function of component 2 luminance (left) or component 2 angle offset relative to component 1 (right). Error bars enclose the 95% confidence interval of the mean. Data points in (*A*) and (*B*) consist on the average of 24 and 30 trials, respectively.

component 2 was varied (Fig. 5*B*). For this paradigm, oscillation frequency rapidly increased from 58 to 68 Hz. Notice that in this case the frequency shift progression was highly nonlinear. For direction offsets greater than 20°, the frequency shift was near its asymptotic value. When the 2 components were presented in opposing directions, however, oscillation frequency was similar to the one observed for the gratings. These observations are consistent with the MUA data (Fig. 4*B*).

Control experiments were made for the confounding effects of stimulus spatial frequency and velocity (Supplementary Material, Fig. 4). It has been shown for the visual cortex in humans that gamma oscillation frequency depends on the spatial frequency of grating stimuli (Hadjipapas et al. 2007). To exclude the possibility that our frequency shift effects could be explained simply by an increase in spatial frequency upon the appearance of component 2, we computed tuning curves for gamma power of the LFP as function of stimulus spatial frequency (see in Supplementary Fig. 4*A* a representative example from a total of 5 sites studied). Our results show that the spatial frequency had a profound effect on both the gamma strength and on the firing rates (one-way ANOVA, $F(5, 232) = 32.3$; $P < 10^{-6}$ and $F(5, 232) = 86.5$, $P < 10^{-6}$, respectively). A control experiment using sinusoidal gratings showed similar results (data not shown). Despite the impact of spatial frequency on gamma power we observed, however, only a minor effect on oscillation frequency, in disagreement with the work of Hadjipapas et al. (2007). Even though we could measure a significant effect on the oscillation frequency (one-way ANOVA, $F(5, 232) = 3.3$; $P = 0.0061$), this could explain only 5% of its variance ($\omega^2 = 0.047$). In any case, the frequency shifts we observed for the plaids were clearly above the effects resulting from changes in spatial frequency.

A remaining concern was stimulus velocity. It is known that the speed of grating stimuli has an effect on the gamma oscillation frequency (Gray et al. 1990; Friedman-Hill et al. 2000; see also our Supplementary Fig. 4*B*). Thus, our frequency shift effects might have been due to changes in speed, because the intersections of plaid stimuli may have higher velocities than the individual components (Adelson and Movshon 1982). We have 2 reasons to exclude this possibility. First, we did see shifts in oscillation frequency even for plaids with intersections moving at the same speed as the individual components (*t*-test,

Downloaded from cercor.oxfordjournals.org at Stadt und Universitatsbibliothek / Section Medizinische Hauptbibliothek on November 12, 2010

df = 153, $P < 10^{-5}$; see in Supplementary Fig. 4*B* a representative example from a total of 4 sites studied). For this, we constructed plaids of orthogonal surfaces, in which only component 1 moved. Second, in the experiments where the direction offset between the components was systematically varied (Figs 4*B* and 5*B*), stimulus velocity appeared not to be correlated with oscillation frequency. As documented in Figure 5*B*, plaid stimuli with small offsets, and thus higher resultant velocities (Movshon et al. 1985), led to smaller shifts in frequency. This trend is opposite to that derived from speed tuning curves (Supplementary Fig. 4*B*).

Gamma Signatures

The stimulus per se was not the only determinant of the gamma oscillation frequency. When we compared data simultaneously acquired from the regions of the central and the peripheral representation of the visual field (operculum, ~3°; calcarine sulcus, ~10° eccentricity), we found that the oscillation frequency was systematically lower for the periphery. Note that the stimulus was the same for both recording sites. Examples are shown in Figure 6*A* separately for responses to

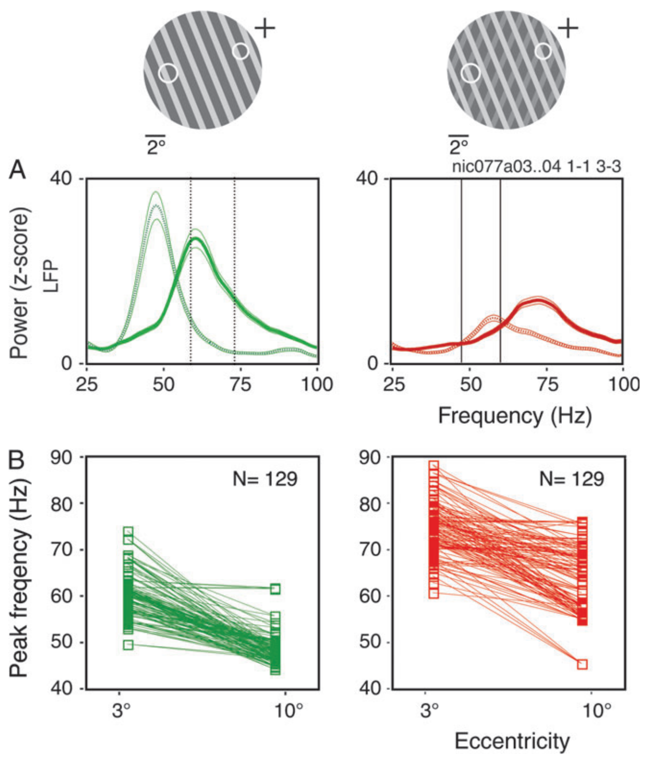

Figure 6. Relation between RF eccentricity and oscillation frequency of the LFP. (*A*) Simultaneously recorded neurons with RFs at central and peripheral regions of the visual field (RFs are indicated by circles and the fixation point by a cross) were stimulated by the same grating (left panel) or plaid (right panel) stimulus (Monkey 1). Central sites refer to ~3° eccentricity and are represented by the continuous curves on both panels. Peripheral sites refer to ~10° eccentricity and is represented by the dotted curves. Higher eccentricities induced lower frequencies, whereas the plaids continued to induce higher frequencies than the gratings for a given eccentricity. Thin traces enclose the 95% confidence interval of the mean. Vertical lines depict the peak frequency: Continuous lines for the gratings and dotted lines for the plaids. (*B*) Population data for all electrode pairs ($n = 129$) simultaneously recorded at central and peripheral sites. Straight lines link data points simultaneously acquired, confirming the overall trend described for the single case shown in (*A*). Each curve (*A*) or data point (*B*) is the average across the 16 directions of movement.

gratings and plaids. Because oscillation frequency was independent of stimulus orientation, data from all conditions were pooled. For responses to gratings, oscillation frequency was 60 Hz for the operculum and 47 Hz for the calcarine sulcus. This amounts to a difference of 13 Hz (21% lower). For responses to the plaids, frequencies were 73 Hz and 58 Hz, for the operculum and calcarine sulcus, respectively (20% lower). This would represent for a 20-ms oscillation cycle (50 Hz) a difference of about 5 ms (90° of the gamma cycle). In the analysis of population data (129 pairs of recording sites, Fig. 6*B*), the differences were highly significant (paired *t*-test, df = 128, $P < 10^{-6}$). Notice that these differences in frequency exist independently of variations due to the stimulus (plaids generally induce higher frequencies than gratings). For a given stimulus, the magnitude of change was about the same for the different eccentricities.

In this study, we obtained data from V1 of the 2 hemispheres in 3 out of the 4 monkeys studied. Comparisons across monkeys revealed surprisingly high variability in the frequency distribution of the LFP (Fig. 7). In responses to gratings at the preferred direction (comparable stimulus size, spatial frequency, and speed), the peak frequency at the gamma band varied approximately 2-fold across the monkeys, from 30 to 65 Hz. A similar variance was also seen for responses to plaids, from 32 to 76 Hz. Importantly, comparisons across the 2 hemispheres of the same monkey revealed a surprising similarity in the frequency distributions. For Monkey 1, although there were large differences in peak width, frequencies were matched across hemispheres (quantitative measures are given in Table 2). Observe that in this monkey there was no attenuation in the average power of gamma oscillations for the plaids. In addition, peaks in the alpha range were consistently visible across the 2 hemispheres. For Monkey 2, we observed the lowest gamma-band frequencies for both the gratings and the plaids. For Monkey 3, the peaks were narrow and consistent across the 2 hemispheres. Notice the strong reduction of power for responses to the plaids (Monkeys 2 and 3). Overall, these results indicate that different individuals differ with respect to the frequency range of gamma processes, which could be viewed as a spectral signature related to the functional architecture of the cortex.

Segmentation of Surfaces

An important goal of our study was to examine whether gamma synchronization contributes to the segmentation of surfaces in V1. The bulk of our experiments was designed to test specifically whether ensembles responding to the same surface remained stable after being challenged by a second surface in a condition associated with perceptual segmentation. Therefore, we have used depth-ordered plaids in most of the experiments. Here we provide additional data for transparent and pattern plaids. Different stimulus configurations were obtained by varying the luminance of the intersections. The plaid stimuli were constructed in a way that at least one of its components matched the tuning properties of the cells. In Figure 8 (Monkey 3), we show a case of spectral analysis obtained for cells recorded from the same electrode. Because in this case the cells were responding to the same component, one expected to see a persistence of oscillatory patterning to all plaid configurations, as it was predicted by Castelo-Branco et al. (2000a). In disagreement with this hypothesis, power and

Downloaded from cercor.oxfordjournals.org at Stadt und Universitatsbibliothek / Section Medizinische Hauptbibliothek on November 12, 2010

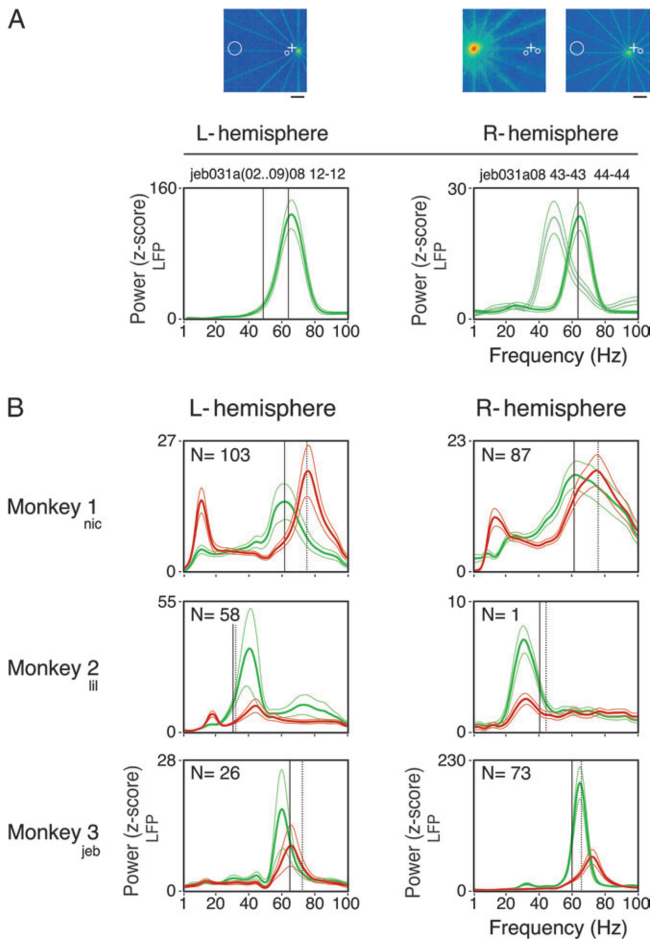

Figure 7. Spectral signatures. (*A*) Comparison of LFP power across the 2 hemispheres (e.g., from Monkey 3). The RF maps for the 3 simultaneously recorded sites in area V1 are plotted above (scale bar, 4°). Warmer colors, representing higher firing rates, reflect the center and extent of each RF. The fixation point position is indicated by a white cross in each map. The 2 central sites (electrodes 1 and 2 for the left and right hemispheres, respectively) were recorded at ~2° eccentricity. Electrode 3 was recorded from the calcarine sulcus of the right hemisphere (~25° eccentricity). Observe that both central sites have similar oscillation frequencies (~64 Hz), which are considerably higher than the one observed at the peripheral site (~49 Hz). (*B*) Comparisons across monkeys. Even though the stimuli employed in all cases were physically similar, each subject had a characteristic spectral profile. In particular, each subject had a dominant gamma frequency for the grating (green curves), stable across recording sessions and hemispheres. Independent of the frequency induced by component 1, the appearance of component 2 increased the peak gamma frequency (red curves). L and R stand for left and right hemispheres, respectively. Each curve is the average of *N* recordings sites as stated on the top-left corner of each plot. Only those sites recorded in the operculum were included in this analysis, with the exception of Monkey 2 (right hemisphere) where the only site recorded was obtained in the calcarine sulcus. Observe that the gamma peaks were rather narrow, showing that increases in gamma activity could not be attributed to shifts of a 1/f spectral distribution. The thinner traces enclose the 95% confidence interval of the mean. Vertical guidelines were positioned to help localize the induced gamma frequency for the corresponding stimulus in the opposite hemisphere: continuous lines for the grating and dotted lines for the plaids. Plaids were depth-ordered.

coherence analysis showed a complete disruption for the transparent and pattern configurations. For the depth-ordered plaid, there was a clear reduction in the LFP power and the LFP–MUA coherence, as described previously. Overall, these results suggest that the heterogenous activation of the cortex may have profound consequences to the generation of gamma oscillations, independent of the stimulus coherence per se.

Table 2
Peak gamma oscillation frequencies for the grating and plaid stimuli across monkeys and hemispheres and the *P* value associated with the peak difference between both stimuli

	Gratings (C1)	Plaids (C1 + C2)	*P* (paired *t*-test)
(A) Left hemisphere			
Monkey 1	62.1 Hz	76.1 Hz	$<10^{-6}$
Monkey 2	40.5 Hz	44.4 Hz	0.0026
Monkey 3	60.1 Hz	65.6 Hz	0.013
Monkey 4	46.1 Hz	55.9 Hz	0.032
(B) Right hemisphere			
Monkey 1	62.2 Hz	75.1 Hz	$<10^{-6}$
Monkey 2	30.7 Hz	32.2 Hz	n/a[a]
Monkey 3	65.1 Hz	72.5 Hz	$<10^{-6}$

[a]Only one site recorded.

Figure 9 shows an example of recordings with overlapping and nonoverlapping RFs obtained from different electrodes at the operculum and the calcarine sulcus. In this case, each component of the plaids matched the properties of a pair of cells. With this configuration we expected to see synchronization of oscillatory responses to the individual components only for the coherent stimulus, that is, the pattern plaids (Castelo-Branco et al. 2000a). Coherence estimates gave different results for the LFP and MUA data. Figure 9*A* displays the LFP power computed for the 3 sites. Notice that there was a selective increase in power for single gratings that matched the orientation preferences of the cells (as measured by the area corresponding to the gamma band, from 30 to 90 Hz). In response to the 2 superimposed components, gamma was strongly attenuated, consistent with our previous observations. In the case of the pattern plaids, however, this attenuation was less pronounced for the LFP power and LFP–LFP coherence. Shifts in oscillation frequency, nevertheless, were present in all cases, indicating the emergence of a new network dynamics. In Figures 9*B*,*C*, coherence analysis is shown for short (1–2 cell pair, overlapping RFs) and long distances (1–3 cell pair, nonoverlapping RFs), respectively. For responses to the pattern plaids (coherent stimulus), the LFP–LFP coherence exhibited robust peaks at 70 Hz that did not decay with distance (peaks for the 1–2 and the 1–3 pairs were equally high). For responses to the noncoherent stimuli (depth-ordered and transparent plaids), on the other hand, the coherence was significantly lower as compared with the coherent stimulus (jackknife procedure of Arvesen, $P < 0.05$ for 65–75 Hz). These results could be interpreted as strong evidence for the synchronization hypothesis, because coherence measures are indicators of precise phase-locking of oscillatory responses (Womelsdorf et al. 2007). In accord with this notion, for cases where the LFP–LFP coherence was high, one would expect to see similarly high values for the MUA–LFP (spike-field) coherence. This was not the case in our data. As shown in Figures 9*B*,*C*, the MUA–LFP coherence was equally flat for all plaid configurations, irrespective of the perceptual coherence of the stimulus. The MUA–MUA coherence (data not shown) was also flat for all conditions.

Selective Attention

A common criticism of the use of a fixation task for studying perceptual mechanisms is that there is no attentional engagement with the stimulus. To address this issue we have designed a series of experiments in which one monkey (Monkey 3) was trained to selectively respond to changes in one of the

Downloaded from cercor.oxfordjournals.org at Stadt und Universitatsbibliothek / Section Medizinische Hauptbibliothek on November 12, 2010

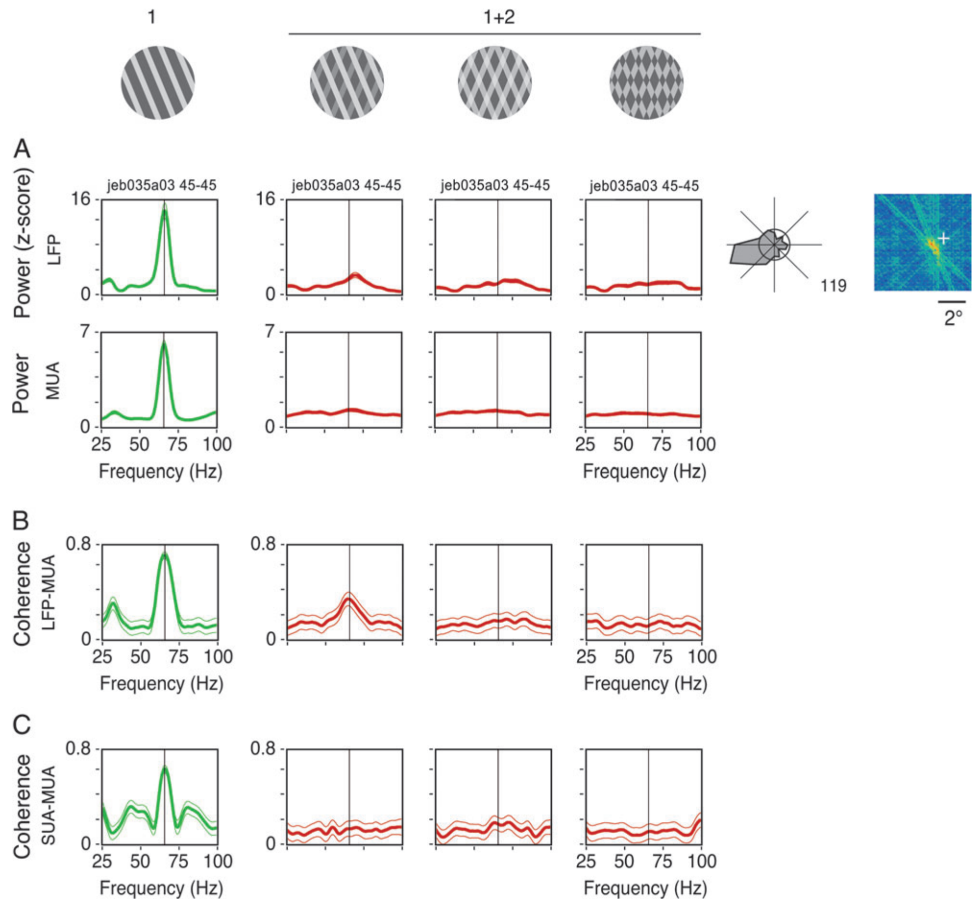

Figure 8. Relations between synchrony and stimulus coherence for recordings obtained from the same electrode. Plaid stimuli (1 + 2) were displayed in the following configurations: depth-ordered, transparent, and pattern plaids (columns from left to right). Depth-ordered and transparent plaids had physical properties compatible with perception of noncoherent motion, whereas the pattern plaid was compatible with perception of coherent motion. (*A*) Spectral power of the LFP (*z*-score) and MUA computed for each stimulus configurations (Monkey 3). (*B*) LFP–MUA coherence. (*C*) As in (*B*), but for SUA–MUA obtained from the same electrode. From a total of 9 cases studied in 2 monkeys, all showed similar results.

components of depth-ordered plaids. In this task, attention was actively maintained on one of the surfaces, while ignoring changes in the other one. The first component to appear was the one to which attention had to be directed to (cued surface). The second component worked as distractor, appearing in front of or behind the first component (details on task timing are given in the Materials and Methods). The component on the foreground (component 1) had always higher luminance as compared with the component on the background (component 2). This was a demanding task, requiring lengthy training. On average, Monkey 3 reached a performance level of 92% correct responses. Spectral and coherence analysis were made for recordings obtained from the opercular region (Fig. 10). Only cells showing clear orientation selectivity were analyzed (31 out of 50 recording sites). As before, the direction of component 1 was chosen to match the preferences of the cells. Analysis windows were placed at 2 epochs: 1) during the responses to the cued surface (first component, gratings) and 2) during the responses after appearance of the distractor surface (component plaids). Observe that for the plaids window, attention had been directed either to the component in the front or to the component in the background. In Figure 10*A* (same recording site as in Fig. 1), an example is shown for attention being directed to the component in the front (component 1). Sliding window analysis of the MUA showed that the onset of the second component led to a nearly complete disruption of the ongoing oscillation. These results are essentially the same as for the passive fixation task (Fig. 1*A*). Spike-triggered averages of the LFP computed for the same data (Supplementary Fig. 5) indicate that the disruption of the oscillatory patterning could not be explained simply by spikes skipping oscillation cycles. Thus, attention was not sufficient to preserve the oscillatory dynamics induced by the gratings, even though perceptually this surface remained unchanged throughout the trial.

A closer analysis of the LFP, however, revealed that our attentional paradigm had a clear effect on the oscillation frequency, indicating that the monkey actually did attend selectively to one of the surfaces. As shown in the power spectra of Figure 10*B*, for average and single trials, the oscillation frequency peaks for the responses to the plaids were clearly different depending on which surface the monkey was attending to. When attention was directed to the foreground (component 1), peak frequencies were ~70 Hz, whereas when it was directed to the background, peaks shifted to ~75 Hz (t-test, df = 48, $P < 10^{-5}$). It is important to emphasize that, for the second analysis window, the stimulus was exactly the same in both conditions. Interestingly, when these

Downloaded from cercor.oxfordjournals.org at Stadt und Universitatsbibliothek / Section Medizinische Hauptbibliothek on November 12, 2010

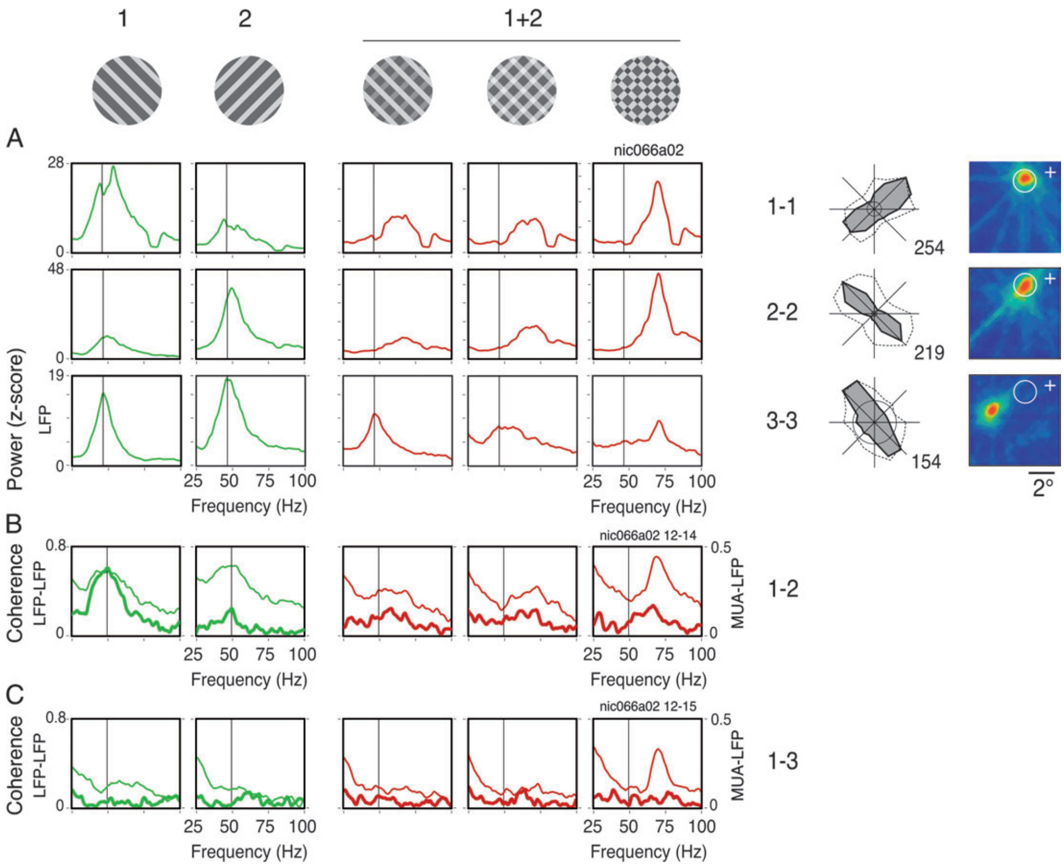

Figure 9. Relations between synchrony and stimulus coherence for recordings obtained from different electrodes (e.g., from Monkey 1). Data shown were obtained for 3 sites recorded simultaneously in area V1 (RF maps are shown to the right, conventions as in Fig. 7). Neurons recorded in the operculum (electrodes 1 and 2, ~3° eccentricity) had overlapping RFs, whereas the RFs of neurons recorded in the calcarine (electrode 3, ~10° eccentricity) were nonoverlapping with those recorded from the operculum. Tuning curves for direction of movement are presented to the left of the RF maps (conventions as in Fig. 1), both for gamma of the LFP (dotted line) and for the spiking responses (solid line). The stimulus used for each condition is shown at the top of each respective column. Direction of motion of components 1 and 2 of the plaids were chosen in accord with the tuning properties of the neurons (component 1 matching the properties of electrode 1 and component 2 matching the properties of electrodes 2 and 3). Plaid stimuli (1 + 2) were displayed in the following configurations: depth-ordered, transparent, and pattern plaids (columns from left to right). Depth-ordered and transparent plaids had physical properties compatible with perception of noncoherent motion, whereas the pattern plaid was compatible with perception of coherent motion. (*A*) Spectral power of the LFP (*z*-score) computed for each condition and recording site. (*B*) LFP–MUA coherence (thick curves) and LFP–LFP coherence (thin curves) computed for the pair of overlapping RF sites (1–2). (*C*) As in (*B*), but for one pair of nonoverlapping RF sites (1–3). From a total of 5 cases studied in 2 monkeys, all showed similar results.

frequencies are compared with the frequency observed for the passive fixation task (72 Hz), we end up with a progression similar to our luminance curve experiment (Fig. 5*A*). As discussed below, this can be understood in view of some current models of attention (Carrasco et al. 2004; Reynolds and Chelazzi 2004). It is possible that selective attention works as a contrast gain mechanism, with impact on surface saliency comparable to our luminance manipulations.

In Figure 10*C* we show results for the comparison between the passive fixation and attentional tasks. There were no significant differences, neither for firing rates (paired t-test, df = 30, $P = 0.22$) nor for MUA–LFP coherence (paired t-test, df = 30, $P = 0.59$). Comparisons for attention to the foreground and to the background surfaces are shown in Figure 10*D*. Note that attentional effects exist only for the oscillation frequency (paired t-test, df = 30, $P < 10^{-6}$).

Discussion

To determine whether synchronous firing in V1 correlates with perceptual segmentation of surfaces, we developed a new paradigm based on plaid stimuli, which enabled us to follow the synchronization dynamics over time. For intersection luminance values compatible with surface segmentation (e.g., nontransparent, depth-ordered plaids), we expected the synchronization patterns induced by single gratings to persist with component plaids. On the contrary, our spectral and coherence analysis of both the LFP and spiking responses revealed profound changes in the ongoing interaction patterns of the neurons. Moreover, the observed changes in synchronization dynamics were not correlated with perceptual coherence of the plaids. As discussed below, these findings are at odds with the notion that different assemblies oscillate in response to different surfaces.

Gamma Responses

In our study, synchronization was generally associated with gamma oscillations. In the cat, it has been shown that cortical states characterized by high levels of EEG activation are associated with high amplitude, sustained gamma oscillations (Herculano-Houzel et al. 1999; Siegel and König 2003), suggesting that synchronization of spiking responses may be facilitated by oscillatory activity. Accordingly, Samonds and Bonds (2005) have shown that for synchronization to be sustained throughout

Downloaded from cercor.oxfordjournals.org at Stadt und Universitatsbibliothek / Section Medizinische Hauptbibliothek on November 12, 2010

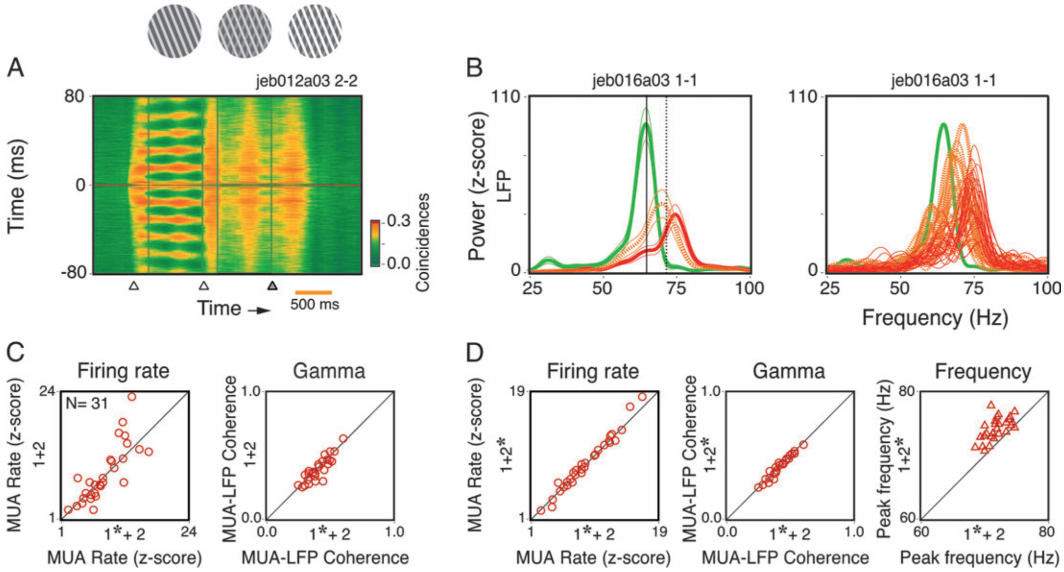

Figure 10. Effects of selective attention to one of the surfaces of the plaids. Monkey 3 was trained to direct attention to the first grating (cue) appearing on the screen. After 1000 ms of cue onset, the second component appeared in front of or behind the first component. The monkey was required to respond with a lever release only when the cued grating changed luminance, ignoring changes on the noncued surface. (*A*) Sliding window autocorrelation of the MUA for the same recording site studied in Figure 1*A*. After the addition of component 2, but with attention directed to component 1, oscillatory activity was still disrupted, similar as to when no attention was payed to the stimulus (Fig. 1). (*B*) LFP spectra for the gratings (green curves) and for the plaids. For the latter case, orange traces represent attention directed to the surface in the foreground, whereas the red traces indicate attention directed to the surface in the background. Continuous and dotted vertical lines indicate the frequency induced by the grating and plaid stimuli, respectively, when attention was directed to the fixation point. Single-trial traces are shown to the right. (*C*) No significant differences in firing rate or spike-field coherence were found depending on whether the monkey was paying attention to the fixation point, to component 1 or to component 2, as shown in (*C*) and (*D*). The * symbol in $1^* + 2$ or $1 + 2^*$ indicates to which component attention was directed to. No symbol ($1 + 2$) indicates that attention was directed to the fixation point. However, the oscillation frequency for the population of sites systematically shifted depending on to which surface the monkey directed its attention to. Thin traces in (*B*), left panel enclose the 95% confidence interval of the mean.

the stimulation period (over seconds), it has to be maintained by oscillatory patterning. In our study, we have rarely seen synchronization without accompanying oscillation, and when it occurred, it was very weak. Maldonado et al. (2000) have found that, for nearly three-quarters of short distance pairs and two-thirds of long distance pairs, synchronization was accompanied by gamma oscillations. Similarly, König et al. (1995b) have shown in the cat that synchronization of responses between sites more than 2-mm apart or between the 2 hemispheres was nearly always associated with oscillatory patterning.

In the present study we have systematically recorded from V1 of the 2 hemispheres in 4 monkeys (3 are shown in Fig. 7). This enabled us to compare oscillation frequencies between individuals across a much larger sample than in previous studies. Comparisons across monkeys revealed surprisingly high interindividual variability in gamma frequency (up to 2-fold). Interhemispheric comparisons, on the other hand, revealed a rather small intraindividual variability. Why such a large variability exists across individuals remains unresolved. Possible explanations are genetic variations in connectivity (Kaschube et al. 2002) and channel kinetics. We have also observed differences in oscillation frequency between sites at the central and the peripheral representation of the visual field in V1. As shown in Figure 6 for pairs of recording sites in the operculum and the calcarine sulcus, oscillation frequency was clearly higher for sites at lower eccentricities. These differences could be attributed to the way stimulus velocity interacts with the cortical magnification factor. It is known that the speed of the visual stimulus has an effect on the oscillation frequency of the cortex: the faster the stimulus, the faster the oscillation (Gray et al. 1990; Friedman-Hill et al. 2000; see also our Supplementary Fig. 4*B*). Because at lower eccentricities the displacement of the stimulus relative to the cortical map is larger, one would expect a faster oscillation. Interestingly, we have observed that for static stimuli, such as Gabor patches set to match the orientation preferences of the cells (Neuenschwander et al. 2008), the oscillation frequency was the same for responses from the operculum and the calcarine sulcus. Differences in oscillation frequency may constrain synchronization for long distances. This may explain our finding of weaker synchronization across sites at central and peripheral representation regions, even for responses to a single coherently moving grating (Supplementary Fig. 3).

It remains an open question how local gamma oscillations in V1 are. Similar to our results (Supplementary Fig. 2), early studies in the cat and in the monkey (Gray and Singer 1989; Frien et al. 2000) have found that the tuning of gamma oscillations in the LFP closely matches the orientation and direction preferences of the local cluster of cells (MUA). It has been argued that the gamma components of the LFP are bound to the scale of a column (Liu and Newsome 2006; Katzner et al. 2009; but see Berens et al. 2008). In our study, we have observed that interactions in V1 are mostly local. As shown in Supplementary Fig. 3, coherence measures for the LFP and MUA decreased steeply as function of cortical distance. Recently, Gieselmann and Thiele (2008) have shown that oscillation strength increases monotonically with stimulus size. Thus, it is possible that gamma patterning requires a critical mass of activity, comprising interactions among several columns.

Breaking the Waves

The main finding of this study was that the coactivation of neuronal populations with different orientation preferences, as

Downloaded from cercor.oxfordjournals.org at Stadt und Universitatsbibliothek / Section Medizinische Hauptbibliothek on November 12, 2010

it occurs for plaid stimuli, led to the disruption of ongoing gamma synchronization. Nonadditive plaid images, as those used in our study, contain Fourier power concentrated at multiple orientation components (Stoner and Albright 1996; see Figure 7*A* of Schmidt et al. 2006). For depth-ordered plaids image, spectral power predominates at one of the components, whereas in pattern plaids power is more evenly distributed, encompassing also components in the intermediate direction. Plaid stimuli, therefore, are capable of activating populations with different orientation preferences, their relative contribution depending on parameters such as angle between the 2 components and luminance values of the individual components and their intersections (Schmidt et al. 2006). In our results, disruption occurred both for pattern and component plaids (Fig. 8), even when the second component had very low contrast (Fig. 4). Thus, a relatively weak activation of other orientation columns was enough to drive the neuronal network into a new dynamical state characterized by near cessation of oscillations in the spiking responses and shifts toward higher oscillation frequencies in the LFP (Fig. 5). These observations were robust and consistent across all monkeys studied.

It is known that the spatial and temporal characteristics of the stimulus can have profound effects on the temporal patterning of the neuronal responses. In a study in the awake cat, Kayser et al. (2003) have shown that the spectral profiles of responses to natural movies are quantitatively and qualitatively different from those to gratings. Whereas gratings induced responses with spectral power largely concentrated at 40 Hz, natural movies led to a uniform increase in power over the whole gamma band and beyond (frequencies above 100 Hz). We have obtained similar results from our recordings in V1 (S.N. and B.L., unpublished observations). Thus, it is likely that complex stimuli, such as plaids and natural scenes, induce fundamentally different patterns of interactions in the cortex, as compared with moving bars or gratings.

Why are gratings so effective in inducing gamma oscillations in the visual cortex? Grating stimuli allow for a steady-state, selective activation of large populations. The very notion of local spatiotemporal filters has been derived from studies using gratings, leading to the Fourier-based approach to vision (Campbell and Robson 1968). Gratings, not surprisingly, have been central for the characterization of orientation domains based on optical imaging techniques (Bonhoeffer and Grinvald 1991). They have also been largely used in investigations on cortical dynamics (e.g., in the monkey, Maldonado et al. 2000; Fries et al. 2001; Gail et al. 2000, 2004; Henrie and Shapley 2005; Womelsdorf et al. 2007). Recently, in a study combining imaging of intrinsic signals and recordings of the LFP, Niessing et al. (2005) found a link between the blood oxygen level-dependent signal and gamma oscillations for responses to full-field gratings. A possible reason for this link is that grating stimuli are capable of activating selectively columns sharing the same properties, which are known to be preferentially connected (Stettler et al. 2002; Schmidt et al. 1997; Weliky et al. 1995; Malach et al. 1993; Gilbert and Wiesel 1989). Cross-correlation analysis has shown that interactions across cells with the same orientation preference are strong, following the layout of the intrinsic horizontal connections (Ts'o et al. 1986; Schwarz and Bolz 1991). Moreover, long-distance gamma synchronization occurs primarily between cells with similar orientation preferences (Engel et al. 1990). In accordance with these previous studies, Smith and Kohn (2008), by means of a high-density sampling of the cortex, have demonstrated that synchronization depends strongly on orientation similarity. Nauhaus et al. (2009) have found that spiking activity triggers traveling waves in the LFP, which propagate long distances in V1 depending on stimulus contrast. Similar to the patterning of horizontal connections, these traveling waves were biased along sites with similar orientation preferences. Thus, it is conceivable that the limit cycle dynamics (narrow-band gamma oscillations) commonly seen in responses to gratings results from cooperative interactions of subpopulations that are preferentially connected.

This does not explain, however, why minimal activation of columns with dissimilar orientation preferences had such a profound impact on the ongoing oscillatory patterns, as shown in Figure 4*A*. This is even more intriguing if one considers that the disruption effect was maximal for the orthogonal orientation offset between the components (Fig. 4*B*). Any explanation for these findings should account for the generation mechanisms of gamma activity, which, as discussed before, seems to be local. It is known from intracellular recordings that local inhibitory networks are key players in the generation of the gamma rhythmicity in the hippocampus and in the cortex (Hasenstaub et al. 2005; Tamás et al. 1998; Whittington et al. 1995; for review see Bartos et al. 2007). Connections across orientation columns are known to be excitatory and inhibitory (Dalva et al. 1997). The concurrent excitatory (or inhibitory) drive from cross-orientation columns apparently interferes with the local generation of the gamma oscillations.

Recently, Zhou et al. (2008) have investigated the impact of stimulus continuity on the modulation of synchronized activity. In responses to gratings onto which noise was superimposed, coherence in the gamma band was impaired, suggesting that spatial continuity is required for the generation of gamma oscillations. Our study offers an alternative interpretation to these results. We observed that the disruption of gamma activity occurred even when the foreground component was left intact and undisturbed. From this perspective, it is possible that the reduction in coherence reported by Zhou et al. (2008) arises because of the activation of cells with dissimilar properties responding to the new orientation components added by the noise.

An important and somehow surprising finding in our study was that the oscillatory patterning of the LFP in response to plaids was dissociated from the spiking activity (Fig. 3*A*). Gieselmann and Thiele (2008) have also reported a dissociation between neuronal firing and LFP activity in area V1. In their study, LFP gamma power was maximal for large grating stimuli covering the surround regions of the RFs, whereas spiking activity showed a clear suppression. It was suggested that the increase in inhibition in the responses to the larger stimuli could be responsible for both the suppression in rates and enhancement of gamma oscillations. We observed, however, no systematic differences in firing rate between the grating and plaid stimuli, despite profound differences in the gamma oscillatory patterning. Thus, it is unlikely that a simple model based on a modulation of inhibition in the cortical network could account for the properties of gamma synchronization we have observed in V1. Another possibility is that the LFP reflects not only activity generated within V1 but also the synaptic activity of reentrant inputs from higher visual areas.

Downloaded from cercor.oxfordjournals.org at Stadt und Universitatsbibliothek / Section Medizinische Hauptbibliothek on November 12, 2010

Scene Segmentation

In early investigations, a common strategy for studying perceptual grouping was to use superimposed objects at different configurations (e.g., 1 single bar vs. 2 crossing bars; Engel et al. 1991; Kreiter and Singer 1996). Castelo-Branco et al. (2000a) generalized these results for the segmentation of surfaces with a paradigm based on plaid stimuli. As in the bar experiments, coherent stimuli (pattern plaids) were associated with synchronization, whereas noncoherent stimuli (component plaids) were not. These results, however, have been recently challenged by a number of studies in the awake behaving monkey, which showed contradictory or negative evidence for the segmentation by synchronization hypothesis (Thiele and Stoner 2003; Roelfsema et al. 2004; Palanca and DeAngelis 2005; Dong et al. 2008).

Contrary to the study of Castelo-Branco et al. (2000a), we found little evidence that synchronization in V1 reflects the global properties of plaid stimuli. For depth-ordered plaids, synchronization should have persisted because component 1 was left unchanged during the whole trial, and the cells continued to respond vigorously to that very surface. Moreover, we expected to see clear differences in synchronization dynamics associated with the perceptual coherence of the stimulus. As shown in Figures 8 and 9, synchronization between the LFP–MUA was equally absent for all plaid configurations. An important difference between our study and the one of Castelo-Branco et al. (2000a) is that, in the anesthetized cat, MUA synchronization occurred without signs of oscillatory patterning of the responses (the LFP was not studied). In a later report, however, Castelo-Branco et al. (2000b) analyzed the oscillatory properties of responses to plaid stimuli and found, as in the present study, that gamma patterning of the responses was prominent for gratings matching the preferences of the cells and nearly absent for the plaids (see also Figure 2*B* of Castelo-Branco et al. 2000a). This happened regardless of the stimulus configuration (coherent or noncoherent plaids), indicating that the oscillations were unlikely to be related to perceptual coherence. In a study using circular gratings, Samonds et al. (2006) also found synchronous firing without oscillations. As in the report of Castelo-Branco et al. (2000b), synchrony (but not the oscillatory patterning per se) reflected stimulus coherence. Thus, in the cat, coactivation of columns with different orientation preferences appears to reduce oscillations but does not necessarily abolish synchrony among nearby columns.

Thiele and Stoner (2003) have designed a behavioral paradigm to test for the role of synchronization on surface segmentation. In their experiments, monkeys were trained to report stimulus coherence, thus enabling a more direct link between neuronal synchronization and perception. Surprisingly, noncoherent plaid stimuli induced more synchronization than did coherent plaids. In their study, however, no LFPs were analyzed, and therefore, it is unknown whether there were changes in oscillatory patterns at the population level. Recently, Palanca and DeAngelis (2005) have used coherence analysis of the MUA and LFP to test for binding of oriented contours in area MT. Essentially, comparisons were made for bar segments presented over the RFs that could belong to the same or to distinct polygon objects. In this paradigm, binding depended on contextual relationships outside the classical RF. Their results showed that synchrony was tightly correlated with RF properties and not to feature grouping per se. As in our study, coherence was much stronger for the LFP than for the MUA and was heavily dependent on the RF overlap and similarity of direction preferences. Thus, it is likely that the functional architecture of the cortex is more determinant of the neuronal synchronization dynamics than previously thought.

In most of our experiments, the monkeys performed a fixation task for which the stimulus was actually ignored. As a control for attentional effects, we trained one monkey to direct attention to one of the surfaces of the plaids, while ignoring the other surface. Similar to the results obtained for the passive fixation task, oscillatory responses to the plaids were also disrupted in the attentional task (Fig. 10*A*). These dramatic changes could not be explained by spikes skipping oscillation cycles (see control in Supplementary Fig. 5). Notably, directing attention to one of the surfaces led to a shift in the oscillation frequency of the LFP, which was similar to that obtained by enhancing the contrast of the second grating (Figs 5*A* and 10*B*, respectively). Selective attention to a stimulus is known to increase its effective contrast or saliency (Carrasco et al. 2004) and may increase the contrast gain of cell responses (Reynolds et al. 2000; Martínez-Trujillo and Treue 2002). Thus, in our study, attending to the foreground surface of the plaids (which had higher luminance) would enhance its effective contrast relative to the background surface (lower luminance). Alternatively, attending to the background surface would decrease the effective contrast between the 2 components, resulting in more interference. Other models, however, such as the response gain or the additive models (Thiele et al. forthcoming), may also account for these effects in V1. These results show that internal states, such as attention, are capable of modulating gamma oscillation frequency. The mechanisms responsible for these dynamical changes are still unknown. In slice preparations, it has been shown that gamma oscillation frequency depends on $GABA_A$ channel conductance and on the decay time constant of inhibitory postsynaptic potentials (Traub et al. 1996; Whittington et al. 1995). It has been shown recently that attention-dependent modulation is stronger for putative inhibitory interneurons (Mitchell et al. 2007). These findings are consistent with the proposal that inhibitory networks, which are central for the generation of gamma oscillations, play an important role in attentional processes (see review in Fries 2009).

The puzzling question remains why we do not see a correlation between synchronization and stimulus coherence, as described for the cat visual cortex (Castelo-Branco et al. 2000a). One reason could be the greater specialization of monkey visual areas as compared with those of the cat. Due to massive expansion of the foveal representation, monkey V1 may be concerned only with the analysis of very local relations, leaving context assessment required for scene segmentation to higher areas. In the cat, on the other hand, global operations could already occur in early areas. This may explain why the only evidence we found for perceptual binding was revealed by the LFP–LFP coherence (Fig. 9*B*,*C*). It is possible that reentrant inputs from higher visual areas represent an important component of LFPs recorded in V1, explaining our apparent dissociation between LFP oscillations and the spiking activity. Interestingly, intracerebral EEG recordings in humans have shown strong modulation of gamma in response to complex stimuli such as faces for the parietal and temporal regions but not for the primary visual cortex (Lachaux et al. 2005). These findings suggest that gamma

Downloaded from cercor.oxfordjournals.org at Stadt und Universitatsbibliothek / Section Medizinische Hauptbibliothek on November 12, 2010

synchronization related to grouping of complex features occurs primarily in higher visual areas, independent of V1 oscillatory patterning.

In conclusion, our results do not support the notion that gamma synchronization in V1 is a correlate of perceptual binding, as it has been suggested in early studies in A17 and A18 of the cat (Engel et al. 1991; Castelo-Branco et al. 2000a) and area MT of the monkey (Kreiter and Singer 1996). On the contrary, our findings indicate that synchronous gamma oscillations in monkey V1 are relatively local, showing only weak phase-locking over long distances (operculum vs. calcarine). In this respect, synchronization of oscillatory responses cannot solve the aperture problem within V1, which probably requires processing in higher areas, with larger RFs and compressed visual field representations, despite the negative evidence found in recent studies in MT (Thiele and Stoner 2003; Palanca and DeAngelis 2005) and V2 (Dong et al. 2008).

Funding

This work has been supported by the Max-Planck Society. B.L. was supported during his doctoral studies by the Graduiertenkolleg, J. W. Goethe University—Frankfurt, the Max-Planck Society, and the Frankfurt Institute for Advanced Studies.

Supplementary Material

Supplementary material can be found at: http://www.cercor.oxfordjournals.org/

Notes

We thank Michaela Klinkmann and Johanna Klon-Lipok for technical assistance and Dr Christiane Kiefert and Clemens Sommers for animal care. We thank Mario Fiorani for the implementation of the RF mapping algorithm, Pascal Fries for introducing us to the multitaper spectral analysis, and to Partha Mitra and collaborators for the Chronux analysis software. Thanks also to Miguel Castelo-Branco, Jerorme Baron, Matthias Munk, and Kerstin Schmidt for insightful discussions and support.
Conflict of Interest: None declared.

Address correspondence to Dr Sergio Neuenschwander, Max-Planck Institute for Brain Research, Deutschordenstrasse 46, 60528 Frankfurt am Main, Germany. Email: neuenschwand@mpih-frankfurt.mpg.de.

References

Adelson EH, Movshon JA. 1982. Phenomenal coherence of moving visual patterns. Nature. 300:523–525.

Bartos M, Vida I, Jonas P. 2007. Synaptic mechanisms of synchronized gamma oscillations in inhibitory interneuron networks. Nat Rev Neurosci. 8:45–56.

Belitski A, Gretton A, Magri C, Murayama Y, Montemurro M, Logothetis N, Panzeri S. 2008. Low-frequency local field potentials and spikes in primary visual cortex convey independent visual information. J Neurosci. 28:5696–5709.

Berens P, Keliris GA, Ecker AS, Logothetis NK, Tolias AS. 2008. Comparing the feature selectivity of the gamma-band of the local field potential and the underlying spiking activity in primate visual cortex. Front Syst Neurosci. 2:1–11.

Bonhoeffer T, Grinvald A. 1991. Iso-orientation domains in cat visual cortex are arranged in pinwheel-like patterns. Nature. 353:429–431.

Buzsáki G, Draguhn A. 2004. Neuronal oscillations in cortical networks. Science. 304:1926–1929.

Campbell FW, Robson JG. 1968. Application of Fourier analysis to the visibility of gratings. J Physiol (Lond). 197:551–566.

Carrasco M, Ling S, Read S. 2004. Attention alters appearance. Nat Neurosci. 7:308–313.

Castelo-Branco M, Goebel R, Neuenschwander S, Singer W. 2000a. Neural synchrony correlates with surface segregation rules. Nature. 405:685–689.

Castelo-Branco M, Neuenschwander S, Goebel R, Singer W. 2000b. Oscillatory firing of neurons in cat visual cortex in response to plaid stimuli. Program No. 251.3 in Abstract Viewer/Itinerary Planner. Society for Neuroscience, New Orleans (LA).

Dalva MB, Weliky M, Katz LC. 1997. Relationships between local synaptic connections and orientation domains in primary visual cortex. Neuron. 19:871–880.

Dong Y, Mihalas S, Qiu F, von der Heydt R, Niebur E. 2008. Synchrony and the binding problem in macaque visual cortex. J Vision. 8: 1–16.

Eckhorn R, Bauer R, Jordan W, Brosch M, Kruse W, Munk M, Reitboeck HJ. 1988. Coherent oscillations: a mechanism of feature linking in the visual cortex? Multiple electrode and correlation analyses in the cat. Biol Cybern. 60:121–130.

Eckhorn R, Frien A, Bauer R, Woelbern T, Kehr H. 1993. High frequency (60–90 Hz) oscillations in primary visual cortex of awake monkey. Neuroreport. 4:243–246.

Engel AK, Fries P, Singer W. 2001. Dynamic predictions: oscillations and synchrony in top-down processing. Nat Rev Neurosci. 2:704–716.

Engel AK, König P, Gray CM, Singer W. 1990. Stimulus-dependent neuronal oscillations in cat visual cortex: inter-columnar interaction as determined by cross-correlation analysis. Eur J Neurosci. 2:588–606.

Engel AK, König P, Singer W. 1991. Direct physiological evidence for scene segmentation by temporal coding. Proc Natl Acad Sci USA. 88:9136–9140.

Friedman-Hill S, Maldonado PE, Gray CM. 2000. Dynamics of striate cortical activity in the alert macaque: I. Incidence and stimulus-dependence of gamma-band neuronal oscillations. Cereb Cortex. 10:1105–1116.

Frien A, Eckhorn R. 2000. Functional coupling shows stronger stimulus dependency for fast oscillations than for low-frequency components in striate cortex of awake monkey. Eur J Neurosci. 12:1466–1478.

Frien A, Eckhorn R, Bauer R, Woelbern T, Gabriel A. 2000. Fast oscillations display sharper orientation tuning than slower components of the same recordings in striate cortex of the awake monkey. Eur J Neurosci. 12:1453–1465.

Fries P. 2005. A mechanism for cognitive dynamics: neuronal communication through neuronal coherence. Trends Cogn Sci. 9:474–480.

Fries P. 2009. Neuronal gamma-band synchronization as a fundamental process in cortical computation. Ann Rev Neurosci. 32:209–224.

Fries P, Nikolić D, Singer W. 2007. The gamma cycle. Trends Neurosci. 30:309–316.

Fries P, Reynolds JH, Rorie AE, Desimone R. 2001. Modulation of oscillatory neuronal synchronization by selective visual attention. Science. 291:1560–1563.

Fries P, Womelsdorf T, Oostenveld R, Desimone R. 2008. The effects of visual stimulation and selective visual attention on rhythmic neuronal synchronization in macaque area V4. J Neurosci. 28:4823–4835.

Gail A, Brinksmeyer HJ, Eckhorn R. 2000. Contour decouples gamma activity across texture representation in monkey striate cortex. Cereb Cortex. 10:840–850.

Gail A, Brinksmeyer HJ, Eckhorn R. 2004. Perception-related modulations of local field potential power and coherence in primary visual cortex of awake monkey during binocular rivalry. Cereb Cortex. 14:300–313.

Gieselmann MA, Thiele A. 2008. Comparison of spatial integration and surround suppression characteristics in spiking activity and the local field potential in macaque V1. Eur J Neurosci. 28: 447–459.

Gilbert CD, Wiesel TN. 1989. Columnar specificity of intrinsic horizontal and corticocortical connections in cat visual cortex. J Neurosci. 9:2432–2442.

Gray CM. 1999. The temporal correlation hypothesis of visual feature integration: still alive and well. Neuron. 24:31–47, 111–125.

Downloaded from cercor.oxfordjournals.org at Stadt und Universitatsbibliothek / Section Medizinische Hauptbibliothek on November 12, 2010

Gray CM, Engel AK, König P, Singer W. 1990. Stimulus-dependent neuronal oscillations in cat visual cortex: receptive field properties and feature dependence. Eur J Neurosci. 2:607–619.

Gray CM, König P, Engel AK, Singer W. 1989. Oscillatory responses in cat visual cortex exhibit inter-columnar synchronization which reflects global stimulus properties. Nature. 338:334–337.

Gray CM, Singer W. 1989. Stimulus-specific neuronal oscillations in orientation columns of cat visual cortex. Proc Natl Acad Sci USA. 86:1698–1702.

Hadjipapas A, Adjamian P, Swettenham JB, Holliday IE, Barnes GR. 2007. Stimuli of varying spatial scale induce gamma activity with distinct temporal characteristics in human visual cortex. Neuroimage. 35:518–530.

Hasenstaub A, Shu Y, Haider B, Kraushaar U, Duque A, McCormick DA. 2005. Inhibitory postsynaptic potentials carry synchronized frequency information in active cortical networks. Neuron. 47:423–435.

Henrie JA, Shapley R. 2005. LFP power spectra in V1 cortex: the graded effect of stimulus contrast. J Neurophysiol. 94:479–490.

Herculano-Houzel S, Munk MH, Neuenschwander S, Singer W. 1999. Precisely synchronized oscillatory firing patterns require electroencephalographic activation. J Neurosci. 19:3992–4010.

Kaschube M, Wolf F, Geisel T, Löwel S. 2002. Genetic influence on quantitative features of neocortical architecture. J Neurosci. 22:7206–7217.

Katzner S, Nauhaus I, Benucci A, Bonin V, Ringach DL, Carandini M. 2009. Local origin of field potentials in visual cortex. Neuron. 61:35–41.

Kayser C, Salazar RF, Konig P. 2003. Responses to natural scenes in cat V1. J Neurophysiol. 90:1910–1920.

Kisvárday ZF, Tóth E, Rausch M, Eysel UT. 1997. Orientation-specific relationship between populations of excitatory and inhibitory lateral connections in the visual cortex of the cat. Cereb Cortex. 7:605–618.

König P. 1994. A method for the quantification of synchrony and oscillatory properties of neuronal activity. J Neurosci Methods. 54:31–37.

König P, Engel AK, Roelfsema PR, Singer W. 1995a. How precise is neuronal synchronization? Neural Comput. 7:469–485.

König P, Engel AK, Singer W. 1995b. Relation between oscillatory activity and long-range synchronization in cat visual cortex. Proc Natl Acad Sci USA. 92:290–294.

Kreiter AK, Singer W. 1996. Stimulus-dependent synchronization of neuronal responses in the visual cortex of the awake macaque monkey. J Neurosci. 16:2381–2396.

Lachaux J-PP, George N, Tallon-Baudry C, Martinerie J, Hugueville L, Minotti L, Kahane P, Renault B. 2005. The many faces of the gamma band response to complex visual stimuli. Neuroimage. 25:491–501.

Lamme VA, Spekreijse H. 1998. Neuronal synchrony does not represent texture segregation. Nature. 396:362–366.

Liu J, Newsome WT. 2006. Local field potential in cortical area MT: stimulus tuning and behavioral correlations. J Neurosci. 26: 7779–7790.

Malach R, Amir Y, Harel M, Grinvald A. 1993. Relationship between intrinsic connections and functional architecture revealed by optical imaging and in vivo targeted biocytin injections in primate striate cortex. Proc Natl Acad Sci USA. 90:10469–10473.

Maldonado PE, Friedman-Hill S, Gray CM. 2000. Dynamics of striate cortical activity in the alert macaque: II. Fast time scale synchronization. Cereb Cortex. 10:1117–1131.

Martínez-Trujillo J, Treue S. 2002. Attentional modulation strength in cortical area MT depends on stimulus contrast. Neuron. 35:365–370.

Matsuda K, Nagami T, Kawano K, Yamane S. 2000. A new system for measuring eye position on a personal computer. Program No. 744.2 in Abstract Viewer/Itinerary Planner. Society for Neuroscience, New Orleans (LA).

Mitchell JF, Sundberg KA, Reynolds JH. 2007. Differential attention-dependent response modulation across cell classes in macaque visual area V1. Neuron. 55:131–141.

Mitra P, Bokil H. 2008. Observed brain dynamics. New York: Oxford University Press.

Movshon JA, Adelson EH, Gizzi MS, Newsome WT. 1985. The analysis of moving visual patterns. In: Chagas C, Gattass R, Gross C, editors. Pattern recognition mechanisms. Vol. 54. Pontificiae Academiae Scientiarum Scripta Varia. Rome: Vatican Press. p. 117–151.

Müller MM, Gruber T, Keil A. 2000. Modulation of induced gamma band activity in the human EEG by attention and visual information processing. Int J Psychophysiol. 38:283–299.

Nauhaus I, Benucci A, Carandini M, Ringach DL. 2009. Stimulus contrast modulates functional connectivity in visual cortex. Nat Neurosci. 12:70–76.

Neuenschwander S, Lima B, Singer W. 2008. Stimulus and task-related gamma oscillations in monkey V1 induced by local and global contours. Program No. 769.24 in Abstract Viewer/Itinerary Planner. Society for Neuroscience, Washington (DC).

Niessing J, Ebisch B, Schmidt KE, Niessing M, Singer W, Galuske RA. 2005. Hemodynamic signals correlate tightly with synchronized gamma oscillations. Science. 309:948–951.

Palanca BJ, Deangelis GC. 2005. Does neuronal synchrony underlie visual feature grouping? Neuron. 46:333–346.

Pesaran B, Pezaris JS, Sahani M, Mitra PP, Andersen RA. 2002. Temporal structure in neuronal activity during working memory in macaque parietal cortex. Nat Neurosci. 5:805–811.

Reynolds JH, Chelazzi L. 2004. Attentional modulation of visual processing. Ann Rev Neurosci. 27:611–647.

Reynolds JH, Pasternak T, Desimone R. 2000. Attention increases sensitivity of V4 neurons. Neuron. 26:703–714.

Roelfsema PR, Lamme VA, Spekreijse H. 2004. Synchrony and covariation of firing rates in the primary visual cortex during contour grouping. Nat Neurosci. 7:982–991.

Rols G, Tallon-Baudry C, Girard P, Bertrand O, Bullier J. 2001. Cortical mapping of gamma oscillations in areas V1 and V4 of the macaque monkey. Vis Neurosci. 18:527–540.

Samonds JM, Bonds AB. 2005. Gamma oscillation maintains stimulus structure-dependent synchronization in cat visual cortex. J Neurophysiol. 93:223–236.

Samonds JM, Zhou Z, Bernard MR, Bonds AB. 2006. Synchronous activity in cat visual cortex encodes collinear and cocircular contours. J Neurophysiol. 95:2602–2616.

Schmidt KE, Castelo-Branco M, Goebel R, Payne BR, Lomber SG, Galuske RA. 2006. Pattern motion selectivity in population responses of area 18. Eur J Neurosci. 24:2363–2374.

Schmidt KE, Kim DS, Singer W, Bonhoeffer T, Löwel S. 1997. Functional specificity of long-range intrinsic and interhemispheric connections in the visual cortex of strabismic cats. J Neurosci. 17: 5480–5492.

Schwarz C, Bolz J. 1991. Functional specificity of a long-range horizontal connection in cat visual cortex: a cross-correlation study. J Neurosci. 11:2995–3007.

Sehatpour P, Molholm S, Schwartz TH, Mahoney JR, Mehta AD, Javitt DC, Stanton PK, Foxe JJ. 2008. A human intracranial study of long-range oscillatory coherence across a frontal-occipital-hippocampal brain network during visual object processing. Proc Natl Acad Sci USA. 105:4399–4404.

Siegel M, König P. 2003. A functional gamma-band defined by stimulus-dependent synchronization in area 18 of awake behaving cats. J Neurosci. 23:4251–4260.

Singer W. 1999. Neuronal synchrony: a versatile code for the definition of relations? Neuron. 24:49–65,111–125.

Smith MA, Kohn A. 2008. Spatial and temporal scales of neuronal correlation in primary visual cortex. J Neurosci. 28:12591–12603.

Stettler DD, Das A, Bennett J, Gilbert CD. 2002. Lateral connectivity and contextual interactions in macaque primary visual cortex. Neuron. 36:739–750.

Stoner GR, Albright TD. 1996. The interpretation of visual motion: evidence for surface segmentation mechanisms. Vision Res. 36:1291–1310.

Tallon-Baudry C, Bertrand O. 1999. Oscillatory gamma activity in humans and its role in object representation. Trends Cogn Sci. 3:151–162.

Tamás G, Somogyi P, Buhl EH. 1998. Differentially interconnected networks of GABAergic interneurons in the visual cortex of the cat. J Neurosci. 18:4255–4270.

Downloaded from cercor.oxfordjournals.org at Stadt und Universitatsbibliothek / Section Medizinische Hauptbibliothek on November 12, 2010

Taylor K, Mandon S, Freiwald WA, Kreiter AK. 2005. Coherent oscillatory activity in monkey area V4 predicts successful allocation of attention. Cereb Cortex. 15:1424–1437.

Thiele A, Pooresmaeili A, Delicato LS, Herrero JL, Roelfsema PR. forthcoming Additive effects of attention and stimulus contrast in primary visual cortex. Cereb Cortex. doi:10.1093/cercor/bhp070.

Thiele A, Stoner G. 2003. Neuronal synchrony does not correlate with motion coherence in cortical area MT. Nature. 421:366–370.

Thomson DJ. 1982. Spectrum estimation and harmonic analysis. Proc IEEE. 70:1055–1096.

Traub RD, Whittington MA, Colling SB, Buzsáki G, Jefferys JG. 1996. Analysis of gamma rhythms in the rat hippocampus in vitro and in vivo. J Physiol. 493:471–484.

Ts'o DY, Gilbert CD, Wiesel TN. 1986. Relationships between horizontal interactions and functional architecture in cat striate cortex as revealed by cross-correlation analysis. J Neurosci. 6:1160–1170.

Varela F, Lachaux JP, Rodriguez E, Martinerie J. 2001. The brainweb: phase synchronization and large-scale integration. Nat Rev Neurosci. 2:229–239.

Vidal JR, Chaumon M, O'Regan JK, Tallon-Baudry C. 2006. Visual grouping and the focusing of attention induce gamma-band oscillations at different frequencies in human magnetoencephalogram signals. J Cog Neurosci. 18:1850–1862.

Weliky M, Kandler K, Fitzpatrick D, Katz LC. 1995. Patterns of excitation and inhibition evoked by horizontal connections in visual cortex share a common relationship to orientation columns. Neuron. 15:541–552.

Whittington MA, Traub RD, Jefferys JG. 1995. Synchronized oscillations in interneuron networks driven by metabotropic glutamate receptor activation. Nature. 373:612–615.

Woelbern T, Eckhorn R, Frien A, Bauer R. 2002. Perceptual grouping correlates with short synchronization in monkey prestriate cortex. Neuroreport. 13:1881–1886.

Womelsdorf T, Fries P, Mitra PP, Desimone R. 2006. Gamma-band synchronization in visual cortex predicts speed of change detection. Nature. 439:733–736.

Womelsdorf T, Schoffelen JM, Oostenveld R, Singer W, Desimone R, Engel AK, Fries P. 2007. Modulation of neuronal interactions through neuronal synchronization. Science. 316:1609–1612.

Zhou Z, Bernard MR, Bonds AB. 2008. Deconstruction of spatial integrity in visual stimulus detected by modulation of synchronized activity in cat visual cortex. J Neurosci. 28:3759–3768.

Downloaded from cercor.oxfordjournals.org at Stadt und Universitatsbibliothek / Section Medizinische Hauptbibliothek on November 12, 2010